JHEP

Published by IOP Publishing for SISSA

Received: *September 30, 2008*
Accepted: *October 27, 2008*
Published: *November 17, 2008*

Sflavor mixing map viewed from a high scale in supersymmetric SU(5)

Pyungwon Ko

School of Physics, KIAS,
Cheongnyangni-dong, Seoul, 130-722, Korea
E-mail: pko@kias.re.kr

Jae-hyeon Park

INFN, Sezione di Padova,
via F Marzolo 8, I-35131, Padova, Italy
E-mail: jae-hyeon.park@pd.infn.it

Masahiro Yamaguchi

Department of Physics, Tohoku University,
Sendai 980-8578, Japan
E-mail: yama@tuhep.phys.tohoku.ac.jp

Abstract: We study flavor violation in a supersymmetric SU(5) grand unification scenario in a model-independent way employing mass insertions. We examine how the quark and the lepton sector observables restrict sfermion mixings. With a low soft scalar mass, a lepton flavor violating process provides a stringent constraint on the flavor structure of right-handed down-type squarks. In particular, $\mu \to e\gamma$ turns out to be highly susceptible to the 1-3 and 2-3 mixings thereof, due to the radiative correction from the top Yukawa coupling to the scalar mass terms of **10**. With a higher scalar mass around the optimal value, in contrast, the quark sector inputs such as B-meson mixings and hadron electric dipole moment, essentially determine the room for sfermion mixing. We also discuss the recent deviation observed in B_s mixing phase, projected sensitivity of forthcoming experiments, and ways to maintain the power of leptonic restrictions even after incorporating a solution to fix the incorrect quark-lepton mass relations.

Keywords: Supersymmetric Standard Model, B-Physics, CP violation, GUT.

JHEP11(2008)051

Contents

JHEP11(2008)051

1. Introduction

The Large Hadron Collider (LHC) has started finally, which we hope will be the first machine to produce supersymmetric particles directly. At this stage, experimental input that is still playing a major role in probing the soft supersymmetry breaking sector and that will keep doing so even in the LHC era, is the flavor changing neutral current (FCNC) and CP violating processes. From this data, one can extract information on the potential new sources of flavor and CP violations in the soft supersymmetry breaking terms (see e.g. [1] and papers that cite it). A model of supersymmetry breaking/mediation, possibly in conjunction with a model of flavor, should be compatible with this information. In particular, the past two years have seen new measurements of B_s-$\overline{B_s}$ mixing, both its size [2, 3] and its phase [4 – 6] (the latter still with low precision), which provide new important restrictions on the mixing between the second and the third families of down-type squarks [7 – 10]. On the other hand, a new experiment is going to explore the lepton flavor violation (LFV) decay mode $\mu \to e\gamma$, squeezing its branching ratio down to the level of 10^{-13} [11], two orders of magnitude lower than the current upper bound. Therefore, it can be regarded as timely to update an analysis on supersymmetric flavor violation.

An interesting option in this style of model-independent analysis is to work with a grand unified theory (GUT). We take the SU(5) group for example. Since a single irreducible representation contains both quarks and leptons, their flavor structures are related. This enables us to use both quark sector and lepton sector processes to look into a single source of flavor violation. It is entertaining to see which observable is supplying a tighter constraint. The outcome can serve as a hint concerning which sector has a higher prospect for discovery of FCNC mediated by sparticles. For the scalar masses and trilinear couplings to obey the GUT symmetry, the scale of supersymmetry breaking mediation should be higher than the GUT scale. We suppose that this scale M_* is given by the reduced Planck scale $M_{\rm Pl}/\sqrt{8\pi} \sim 2 \times 10^{18}$ GeV, or very close to it, as is the case in a gravity mediation scenario.

This work is by no means the first attempt in this direction [12 – 18]. Most notably, there is a recent article that has performed an analysis in a similar framework [16]. Three differences are worth mentioning. First, we use the aforementioned $\mu \to e\gamma$ decay mode to constrain the 1-3 and the 2-3 mixings, in addition to $\tau \to e\gamma$ and $\tau \to \mu\gamma$ which were considered in ref. [16]. This seemingly unrelated process becomes relevant, and highly restrictive in some cases, thanks to the radiative correction to the **10** representation scalar mass matrix from the top Yukawa coupling and the Cabibbo-Kobayashi-Maskawa (CKM) mixing [19]. As a matter of fact, this mechanism has long been known and included in many of the preceding model studies [12, 20, 21]. Yet, this is the first instance of taking it into account in a model independent analysis allowing for general flavor mixing of sfermions, as far as we know. Second, the authors of ref. [16] assume that the quark and the lepton mass eigenstates at the GUT scale are aligned to a high degree. This may or may not be the case if a solution is incorporated for fixing the wrong quark-lepton mass relations. Especially, the first and the second families are subject to unlimited misalignment in general [12]. We propose a method to overcome this obstacle to some extent. Third, we elucidate the importance of the gaugino to scalar mass ratio as a key parameter governing relative strengths of the hadronic and the leptonic flavor violations. We show expansions and shrinks of the territory ruled by each of the two sectors. In addition to these refinements, we include remarks concerning the latest hint of anomaly in the mixing phase of the B_s-meson [22, 23].

This paper is organized as follows. In section 2, we spell out basics of flavor physics in a supersymmetric SU(5) GUT model. Section 3 presents the procedure of numerical analysis and the experimental inputs. In section 4, we exhibit the exclusion plot of each mass insertion, and discuss how one can interpret the plot conservatively when the lagrangian has non-renormalizable terms for accommodating the first and the second family fermion masses. This section also has a collection of upper bounds on the sfermion mixings, as well as deviations in selected CP asymmetries allowed by the other constraints. With a summary, we conclude in section 5. One can find notations of the soft supersymmetry breaking terms and the mass insertion parameters in the appendix.

2. SU(5) GUT and FCNC

2.1 GUT relation between squark and slepton mixings

Let us begin by reviewing basic elements of a supersymmetric SU(5) grand unification model, that are relevant to flavor physics. The superpotential has the Yukawa couplings

and the right-handed neutrino mass terms,

$$W_{\rm GUT} \supset -\frac{1}{4}\epsilon_{abcde}\lambda_U^{ij}T_i^{ab}T_j^{cd}H^e + \sqrt{2}\,\lambda_D^{ij}\overline{H}_a T_i^{ab}\overline{F}_{jb} - \lambda_N^{ij}N_i\overline{F}_{ja}H^a + \frac{1}{2}M_N^{ij}N_iN_j. \quad (2.1)$$

Matter fields in **10** and $\overline{\mathbf{5}}$ representations are denoted by T and $\overline{F}$, respectively, **5** and $\overline{\mathbf{5}}$ Higgses by H and $\overline{H}$, respectively, and a right-handed neutrino by N. The indices $a,\ldots,e$ run over components of the fundamental representation of SU(5), and $i,j=1,2,3$ indicate the family. Obviously, λ_U and M_N are symmetric matrices while λ_D and λ_N are not. The above Yukawa couplings, by themselves, predict mass unification of down-type quarks and charged leptons at the GUT scale:

$$m_e = m_d, \quad m_\mu = m_s, \quad m_\tau = m_b. \quad (2.2)$$

Among these, the third relation is consistent with measurements at low energies, while the first two are not. One way to explain this discrepancy is to make corrections to relatively smaller masses by including the following non-renormalizable terms [24]:

$$\begin{aligned} W_{\rm NR} = {} & \frac{1}{4}\epsilon_{abcde}\left(f_1^{ij}T_i^{ab}T_j^{cd}\frac{\Sigma_f^e}{M_*}H^f + f_2^{ij}T_i^{ab}T_j^{cf}H^d\frac{\Sigma_f^e}{M_*}\right) \\ & + \sqrt{2}\left(h_1^{ij}\overline{H}_a\frac{\Sigma_b^a}{M_*}T_i^{bc}\overline{F}_{jc} + h_2^{ij}\overline{H}_a T_i^{ab}\frac{\Sigma_b^c}{M_*}\overline{F}_{jc}\right) + h_N^{ij}N_i\overline{F}_{ja}\frac{\Sigma_b^a}{M_*}H^b, \end{aligned} \quad (2.3)$$

where Σ is the adjoint Higgs multiplet responsible for breaking SU(5) down to the Standard Model (SM) gauge group. These terms will contribute to the Yukawa couplings of the effective theory below the GUT scale, expressed in terms of the SM fields as

$$W_{\rm SSM} = Q^T Y_U \overline{U} H_u + Q^T Y_D \overline{D} H_d + L^T Y_E \overline{E} H_d + L^T Y_N N H_u + \frac{1}{2}N^T M_N N, \quad (2.4)$$

where the fields denoted by uppercase letters are components of the GUT multiplets,

$$T_i \simeq \{Q, \overline{U}, \overline{E}\}_i, \quad \overline{F}_i \simeq \{\overline{D}, L\}_i. \quad (2.5)$$

The Yukawa couplings appearing in the superpotential of (2.4) are related to those in (2.1) and (2.3) by

$$Y_U = \lambda_U + \xi\left(\frac{3}{5}f_1 + \frac{3}{20}f_2^S + \frac{1}{4}f_2^A\right), \quad (2.6a)$$

$$Y_D = \lambda_D - \xi\left(\frac{3}{5}h_1 - \frac{2}{5}h_2\right), \quad (2.6b)$$

$$Y_E^T = \lambda_D - \xi\frac{3}{5}(h_1 + h_2), \quad (2.6c)$$

$$Y_N^T = \lambda_N + \xi\frac{3}{5}h_N, \quad (2.6d)$$

where the superscripts S and A denote the symmetric and the antisymmetric part of the given matrix, respectively. The small number ξ is defined by

$$\xi \equiv 5\frac{\sigma}{M_*} \approx 10^{-2}, \quad (2.7)$$

where σ is the vacuum expectation value (VEV) of Σ, expressed as in

$$\langle \Sigma \rangle = \sigma \, \mathrm{diag}(2, 2, 2, -3, -3). \tag{2.8}$$

The contribution from the non-renormalizable terms makes the difference,

$$Y_D - Y_E^T = \xi h_2, \tag{2.9}$$

and this can account for the first and the second family quark and lepton masses.

For this purpose, ref. [16] does not make use of the $\mathcal{O}(\xi)$ corrections, but they rely on Georgi-Jarlskog mechanism [25]. Their scenario corresponds to a case in our work where the quark and the lepton mass eigenbases coincide, i.e. $U_L = U_R = \mathbf{1}$ in the formalism spelled out below.

Note that the proton lifetime depends on the structure of non-renormalizable operators [26], thereby imposing a restriction on the parameters appearing in (2.3). There are corners of the parameter space in conflict with proton decay experiments. The present work is not specific to a particular pattern of those terms and is valid provided that they are Planck-suppressed.

In order to discuss flavor violation coming from the sfermion sector, one should fix the basis of matter supermultiplets. One can choose a basis of T_i and $\overline{F}_i$ fields such that

$$Y_U = V_Q^T \widehat{Y}_U U_Q^*, \quad Y_D = \widehat{Y}_D, \quad Y_E = U_L^T \widehat{Y}_E U_R^*, \quad Y_N = U_L^T V_L^T \widehat{Y}_N, \tag{2.10}$$

where the hat on a matrix signifies that the given matrix is diagonal with positive elements [27], V_Q and V_L are unitary matrices in the standard parametrization [28, 29] each with three mixing angles and one phase, and U_Q, U_L, and U_R are general unitary matrices. Note that Y_U may not be a symmetric matrix, unlike λ_U. In this basis where Y_D is diagonal, Y_E may not be diagonalized in general due to the difference (2.9), and it should be decomposed into the above form using U_L and U_R. These two unitary matrices describe the mismatch between the down-type quark and the charged lepton mass eigenstates, arising from breakdown of the Yukawa unification $Y_E^T = Y_D$ which is a consequence of SU(5) at the renormalizable level. Since U_L and U_R are crucial in correlating hadronic and leptonic processes, we need to examine their structures. We can estimate the size of an off-diagonal element of Y_E in the unit of the tau Yukawa coupling,

$$\frac{Y_E - \widehat{Y}_D}{[\widehat{Y}_E]_{33}} = \frac{-\xi h_2^T}{m_\tau/(v \cos\beta)} \approx -\cos\beta \, h_2^T, \tag{2.11}$$

where $v \simeq 170$ GeV is the Higgs VEV. Notice the suppression by the factor $\cos\beta$ for high $\tan\beta$. Assuming that each element of h_2 is not larger than $\mathcal{O}(1)$, one can obtain approximate magnitudes of 1-3 and 2-3 mixings [12],

$$\begin{aligned} [U_L]_{3a} &\approx -\cos\beta \, [h_2]_{3a}, \quad [U_L]_{a3} \approx \cos\beta \, [U_L h_2^* U_R^\dagger]_{a3}, \\ [U_R]_{3a} &\approx -\cos\beta \, [h_2^\dagger]_{a3}, \quad [U_R]_{a3} \approx \cos\beta \, [U_L^* h_2^T U_R^T]_{3a}, \end{aligned} \tag{2.12}$$

for $a = 1, 2$. Note that they are suppressed by $\cos\beta$. The other entries of U_L and U_R can be of $\mathcal{O}(1)$. Finally, we relate the fields to the down-quark and charged lepton mass eigenstates as

$$Q = q, \quad \overline{U} = U_Q^T \overline{u}, \quad \overline{E} = U_R^T \overline{e}, \quad \overline{D} = \overline{d}, \quad L = U_L^\dagger l. \tag{2.13}$$

This leads us to the superpotential,

$$\begin{aligned} W_{\rm SSM} = {} & q^T [V_Q^T \widehat{Y}_U] \overline{u} H_u + q^T [\widehat{Y}_D] \overline{d} H_d \\ & + l^T [\widehat{Y}_E] \overline{e} H_d + l^T [V_L^T \widehat{Y}_N] N H_u + \frac{1}{2} N^T M_N N. \end{aligned} \tag{2.14}$$

One can notice that V_Q is the CKM matrix at the GUT scale. If M_N is diagonal in this basis, one also has $V_L = U_{\rm PMNS}^\dagger$. Otherwise, the lepton mixing matrix receives additional rotations for diagonalizing M_N.

Let us turn to the soft supersymmetry breaking sector. The SU(5) symmetry relates the soft supersymmetry breaking terms of squarks and sleptons in a single GUT multiplet. The scalar mass terms are given by

$$-\mathcal{L}_{\rm soft} \supset \overline{F}^\dagger m_{\overline{F}}^2 \overline{F} + T^\dagger m_T^2 T + \overline{F}^\dagger \frac{\Sigma}{M_*} m_{\overline{F}}^{2\prime} \overline{F} + T^\dagger \frac{\Sigma}{M_*} m_T^{2\prime} T + \cdots, \tag{2.15}$$

in which the higher dimensional terms involving Σ are suppressed by $\mathcal{O}(\xi)$. In terms of these soft mass parameters of the GUT multiplets, one can express the soft scalar mass matrices of the SM fields as

$$m_Q^2 = m_T^2 + \frac{1}{10}\xi\, m_T^{2\prime}, \qquad m_U^{2*} = m_T^2 - \frac{2}{5}\xi\, m_T^{2\prime}, \qquad m_E^{2*} = m_T^2 + \frac{3}{5}\xi\, m_T^{2\prime}, \tag{2.16a}$$

$$m_D^{2*} = m_{\overline{F}}^2 + \frac{2}{5}\xi\, m_{\overline{F}}^{2\prime}, \qquad m_L^2 = m_{\overline{F}}^2 - \frac{3}{5}\xi\, m_{\overline{F}}^{2\prime}, \tag{2.16b}$$

using (2.5). From these expressions and (2.13), one can see that the mass insertion parameters of down-type squarks and sleptons at the GUT scale are linked by

$$\delta_{LL}^l = U_L\, \delta_{RR}^{d*}\, U_L^\dagger + \mathcal{O}(\xi), \tag{2.17a}$$

$$\delta_{RR}^l = U_R\, \delta_{LL}^{d*}\, U_R^\dagger + \mathcal{O}(\xi). \tag{2.17b}$$

We can notice two possible sources of deviation from the naive equalities [14],

$$\delta_{LL}^l = \delta_{RR}^{d*}, \quad \delta_{RR}^l = \delta_{LL}^{d*}. \tag{2.18}$$

One is the higher dimensional terms in (2.15), which makes the $\mathcal{O}(\xi)$ corrections, and the other is U_L and U_R, the unitary transformations parametrizing the misalignment between the down-type quark and the charged lepton mass eigenstates. The former type of corrections is negligible compared to the typical size of a scanning mass insertion parameter appearing later on. On the other hand, these corrections might be comparable to the renormalization group (RG) contribution to δ_{RR}^l. Unless they are tuned in such a way that they cancel out the RG-generated δ_{RR}^l, they nevertheless do not undermine the importance of $\mu \to e\gamma$ constraint. The latter needs more consideration. Obviously, U_L and U_R depend

on h_2 through Y_E. If h_2 is diagonal in the basis where Y_D is diagonal, U_L and U_R are unit matrices, and (2.18) becomes a fairly good approximation correlating squark and slepton flavor mixings. If h_2 is not diagonal, the correlation gets loose, but in many cases, LFV processes can still give meaningful restrictions on the down-type squark mixings, thanks to the suppression of 1-3 and 2-3 mixings shown in (2.12). Examples of this situation will be presented in section 4.2.

In a similar way, the GUT symmetry links the scalar trilinear coupling terms of squarks and sleptons so that their chirality-flipping mass insertions have the relations,

$$\delta^l_{LR} = U_L\, \delta^{d\,T}_{LR}\, U_R^\dagger + \mathcal{O}(\xi) \times A_0 \langle H_d \rangle / \widetilde{m}^2_{\widetilde{l}}, \tag{2.19}$$

where A_0 is the overall scale of the A-terms and $\widetilde{m}_{\widetilde{l}}$ is the average slepton mass. In what follows, we do not use this expression since we will ignore the A-term contributions to flavor violating processes.

2.2 RG running of scalar masses

RG running from one scale down to a lower scale generates off-diagonal elements of a scalar mass matrix. For our purpose, we need to consider two intervals of scale: from M_* to $M_{\rm GUT}$, and from $M_{\rm GUT}$ (via M_R) to $M_{\rm SUSY}$. The former is needed to determine the boundary condition to give on the soft supersymmetry breaking terms at the GUT scale, and the latter is to connect the given boundary condition with low energy observables.

First, we think of running between M_* and $M_{\rm GUT}$. Using one-loop approximation, the RG-induced off-diagonal elements can be written as [30, 31]

$$\Delta_{\rm g} m_T^2 \simeq -\frac{2}{(4\pi)^2}[3\lambda_U^*\lambda_U^T + 2\lambda_D^*\lambda_D^T](3m_0^2 + |A_0|^2)\ln\frac{M_*}{M_{\rm GUT}}, \tag{2.20a}$$

$$\Delta_{\rm g} m_{\overline{F}}^2 \simeq -\frac{2}{(4\pi)^2}[4\lambda_D^\dagger\lambda_D + \lambda_N^\dagger\lambda_N](3m_0^2 + |A_0|^2)\ln\frac{M_*}{M_{\rm GUT}}, \tag{2.20b}$$

where m_0 is the scalar mass and A_0 is the trilinear scalar coupling. Let us focus on the mass matrix of T fields, which feeds into the mixings of left-handed squarks and right-handed sleptons. From (2.6a), (2.10), (2.16a), and (2.20a), one can obtain the following form of RG contribution to the LL squark mixing at the GUT scale,

$$(\delta^d_{ij})_{LL} \simeq -\frac{6}{(4\pi)^2}\,[V_Q^\dagger \widehat{Y}_U^2 V_Q]_{ij}\,\frac{3m_0^2 + |A_0|^2}{\widetilde{m}^2_{\widetilde{d}}(M_{\rm GUT})}\ln\frac{M_*}{M_{\rm GUT}} + \mathcal{O}(\xi). \tag{2.21}$$

The $\mathcal{O}(\xi)$ correction in the second term is not necessarily smaller than the first term coming from the CKM mixing and the large top quark Yukawa coupling. Neither is it very likely, however, that they cancel out leading to a value much smaller than the first term. That is, the left-handed squark mixing in the above expression, without the $\mathcal{O}(\xi)$ correction, can be regarded as the minimal value of $(\delta^d_{ij})_{LL}$ that is expected in a supersymmetric SU(5) model with the cutoff at M_*. Let us record the CKM matrix dependence of the above minimal mass insertions,

$$(\delta^d_{12})_{LL} \sim V_{td}^* V_{ts} \sim \lambda^5, \quad (\delta^d_{13})_{LL} \sim V_{td}^* V_{tb} \sim \lambda^3, \quad (\delta^d_{23})_{LL} \sim V_{ts}^* V_{tb} \sim \lambda^2, \tag{2.22}$$

JHEP11(2008)051

where we also express them as powers of λ, sine of the Cabibbo angle.

Using (2.17b), one can get the right-handed slepton mixing from (2.21). Again, we drop the $\mathcal{O}(\xi)$ term in (2.17b), assuming that it does not conspire with the first term to result in a drastic cancellation. If U_R is an identity matrix, $(\delta^l_{ij})_{RR}$ has the same pattern as (2.22). Otherwise, one should take the misalignment into account. As (2.12) shows that the 1-3 and 2-3 mixings are suppressed, one can rephrase (2.17b) into

$$(\delta^l_{a3})_{RR} = [U_R]_{ab}\,(\delta^d_{b3})^*_{LL}\,[U_R]^*_{33} + \mathcal{O}(\cos^2\beta\,\delta^d_{LL}), \quad a,b = 1,2, \tag{2.23}$$

where $[U_R]_{ab}$, the upper-left 2×2 submatrix of U_R, is approximately unitary. [Supposing universal scalar masses at M_*, one actually has another term of the form $[U_R]_{a3}\,(\delta^d_{33})_{LL}\,[U_R]^*_{33}$ where (with an abuse of notation what we here call) $(\delta^d_{33})_{LL}$ is given by setting $i=j=3$ in (2.21). In what follows we discard this term although it can be larger than what is kept in the above equation. Even if it happens to be non-negligible, it generically enlarges the rate of $\mu\to e\gamma$, only to reinforce the sensitivity of this LFV channel.] Keeping only the powers of λ, one can schematically rewrite this as

$$(\delta^l_{13})_{RR} \sim [U_R]_{11}\lambda^3 + [U_R]_{12}\lambda^2, \quad (\delta^l_{23})_{RR} \sim [U_R]_{21}\lambda^3 + [U_R]_{22}\lambda^2. \tag{2.24}$$

The mixing between the first and the second families, described by $[U_R]_{ab}$, is not particularly restricted to be small. There can be small, large, or no mixing. One finds that $(\delta^l_{a3})_{RR}$ is generically not much smaller than λ^3, unless the mixing is fine-tuned in such a way that the two terms cancel out in either of (2.24). For example, the mixing angle should be tuned between $-\lambda\pm\lambda^2$ in order to have $|(\delta^l_{13})_{RR}| \lesssim \lambda^4$.

Next, we should turn to the running below $M_{\rm GUT}$. Before examining an off-diagonal entry of a scalar mass matrix, let us recall the running of a diagonal element since a mass insertion parameter is normalized by it. Squark and slepton masses at $M_{\rm SUSY}$ are approximately related to the GUT scale variables by

$$\widetilde{m}^2_{\tilde{d}}(M_{\rm SUSY}) \approx (1+6x)\,m_0^2, \tag{2.25a}$$

$$\widetilde{m}^2_{\tilde{l}}\,(M_{\rm SUSY}) \approx m_0^2, \tag{2.25b}$$

with the definition of gaugino to scalar (squared) mass ratio,

$$x \equiv M^2_{1/2}/m_0^2. \tag{2.26}$$

The squark mass increases considerably by the gaugino mass contribution. The slepton mass actually receives a small correction from the gaugino mass, but it can be ignored for later discussions. These facts will be crucial to understanding parameter dependence of a constraint.

Unless $\tan\beta$ is extremely high, an off-diagonal element of m^2_D does not run significantly, while running of the left-handed squark mass matrix makes the difference [32],

$$\Delta_{\rm s}[m^2_Q]_{ij} \simeq -\frac{2}{(4\pi)^2}\,[V_Q^\dagger \widehat{Y}_U^2 V_Q]_{ij}\,(3m_0^2 + |A_0|^2)\ln\frac{M_{\rm GUT}}{M_{\rm SUSY}}. \tag{2.27}$$

Using these facts and (2.25a), we can associate squark mass insertions at $M_{\rm SUSY}$ to those at $M_{\rm GUT}$ as

$$(\delta^d_{ij})_{RR}(M_{\rm SUSY}) \approx \frac{(\delta^d_{ij})_{RR}(M_{\rm GUT})}{1+6x}, \tag{2.28a}$$

$$(\delta^d_{ij})_{LL}(M_{\rm SUSY}) \approx \frac{(\delta^d_{ij})_{LL}(M_{\rm GUT}) + q_{ij}}{1+6x}, \tag{2.28b}$$

with the definition

$$q_{ij} \equiv \Delta_{\rm s}[m^2_Q]_{ij}/m^2_0. \tag{2.29}$$

In a parallel way, one can relate slepton mass insertions at a low scale to those at a high scale by

$$(\delta^l_{ij})_{RR}(M_{\rm SUSY}) \approx (\delta^l_{ij})_{RR}(M_{\rm GUT}), \tag{2.30a}$$

$$(\delta^l_{ij})_{LL}(M_{\rm SUSY}) \approx (\delta^l_{ij})_{LL}(M_{\rm GUT}) + l_{ij}, \tag{2.30b}$$

using (2.25b) and the definition $l_{ij} \equiv \Delta_{\rm s}[m^2_l]_{ij}/m^2_0$ with the radiative correction to the off-diagonal slepton mass matrix entries [33],

$$\Delta_{\rm s}[m^2_l]_{ij} \simeq -\frac{2}{(4\pi)^2}\,[V_L^\dagger \widehat{Y}_N^2 V_L]_{ij}\,(3m^2_0 + |A_0|^2)\ln\frac{M_{\rm GUT}}{M_R}. \tag{2.31}$$

This estimate is based on the assumption that the right-handed neutrinos are degenerate so that they are integrated out at a single scale M_R. If they are not degenerate, it is modified to involve mixings, phases, and eigenvalues of M_N (see e.g. [13]). Even in this case, it has been shown that one can use the above form of expression by replacing M_R with the largest eigenvalue of M_N, if there is a large hierarchy among the right-handed neutrino masses [13]. Unlike the quark sector, we do not yet have much information on the neutrino Yukawa couplings. They can be of $\mathcal{O}(1)$ in the case of heavy right-handed neutrinos, or extremely small if the neutrino masses are of Dirac type. Even if we suppose that seesaw mechanism is working, a vast range of right-handed neutrino mass scale is possible, from around the GUT scale down to the weak scale. Although the lepton mixing angles have been measured to an extent, they cannot be directly related to the mixing matrix V_L due to the additional degrees of freedom in M_N, the Majorana right-handed neutrino mass matrix. Moreover, the hierarchy of neutrino masses is unknown yet. As the magnitude of l_{ij} in one model can greatly differ from another, we choose to drop it in the following analysis. Therefore, the results shown later are legitimate only for a scenario where right-handed neutrinos are light enough for l_{ij} to be negligible in (2.30b). (For a study on a case with a large neutrino Yukawa coupling and a specific boundary condition on the soft terms, see e.g. [18, 34, 35].)

Nevertheless, there are circumstances where one can tell consequences of non-negligible l_{ij}. Here, we assume that U_L is a unit matrix. This assumption will be relaxed in section 4.2. If neutrino Yukawa couplings are large, they affect not only the running below, but also above $M_{\rm GUT}$, of m^2_l. Thus, $(\delta^l_{ij})_{LL}(M_{\rm GUT})$ is decomposed into two pieces,

$$(\delta^l_{ij})_{LL}(M_{\rm GUT}) \approx (\delta^l_{ij})_{LL}(M_*) + \alpha l_{ij}, \tag{2.32}$$

JHEP11(2008)051

where the first term represents possible flavor non-universality at the reduced Planck scale, and the second is the RG contribution with

$$\alpha \equiv \frac{\ln(M_*/M_{\rm GUT})}{\ln(M_{\rm GUT}/M_R)}. \tag{2.33}$$

What we will do in the following sections is to search for a set of viable values of $(\delta^l_{ij})_{LL}(M_{\rm GUT})$, imposing experimental constraints. In terms of the variables in (2.32), we can interpret this procedure in two different ways: we fix l_{ij} and scan over $(\delta^l_{ij})_{LL}(M_*)$, or the other way around. As an example of the first option, suppose that one studies a neutrino mass model in which the neutrino Yukawa matrix is given, but there is a room for flavor mixing in the soft supersymmetry breaking terms. In this case, one can easily guess the allowed region of $(\delta^l_{ij})_{LL}(M_{\rm GUT}) = (\delta^d_{ij})^*_{RR}(M_{\rm GUT})$ from the one shown in section 4.1 using (2.30b): shift the region by $-l_{ij}$. This method is applicable to a model with non-degenerate right-handed neutrinos as well. Regarding the second option, one can imagine a situation where the only source of $\overline{F}$ mixing is the neutrino Yukawa matrix, i.e. $(\delta^l_{ij})_{LL}(M_*) = 0$. Under this condition, (2.30b) can be rewritten as

$$(\delta^l_{ij})_{LL}(M_{\rm GUT}) \approx \frac{\alpha}{1+\alpha}\,(\delta^l_{ij})_{LL}(M_{\rm SUSY}), \tag{2.34}$$

which relies on the degeneracy of right-handed neutrinos. Obviously, the allowed region of $(\delta^l_{ij})_{LL}(M_{\rm GUT})$ is given by shrinking the one in section 4.1 by the factor $\alpha/(1+\alpha)$.

In this subsection, we used one-loop estimates to understand the qualitative behaviors of squark and slepton mixings, but we numerically solve RG equations for quantitative analysis in the subsequent sections.

3. How to impose constraints on scalar mixings

3.1 Scheme

One popular way to constrain sfermion mixings in a model-independent fashion is to scan over one mass insertion parameter at a time, while setting the other parameters to zero. The practical reason to assume all but one of the parameters to be zero is that it is difficult or impossible to take more than one complex mass insertions as free variables and plot the allowed volume. Despite its makeshift motive, this strategy works as long as the parameter being swept by itself makes the dominant contribution to the process in consideration. However, there are cases where presence of another mass insertion amplifies the contribution from the scanned parameter, thereby rendering the constraint from a process much tighter.

A well known example is $B \to X_s\gamma$. For instance, a single $(\delta^d_{23})_{RR}$ insertion contributes to this decay via the gluino loop shown in figure 1 (a). If one takes into account nonzero $(\delta^d_{33})_{RL}$ insertion as well, the diagram in figure 1 (b) with double insertions can make an additional contribution [10, 36], whose amplitude is enhanced by $\tan\beta$ relative to the single insertion graph due to the chirality flip on the gluino propagator. The reason for including the double insertion diagram, namely considering nonzero $(\delta^d_{33})_{RL}$ in addition to the $(\delta^d_{23})_{RR}$ under inspection, is not only that it can significantly increase the $B \to X_s\gamma$ branching ratio,

JHEP11(2008)051

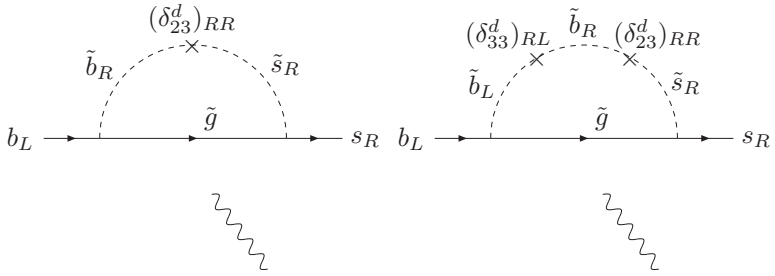

(a) single insertion (b) double insertion

Figure 1: Gluino loop contributions of $(\delta^d_{23})_{RR}$ to $B \to X_s\gamma$.

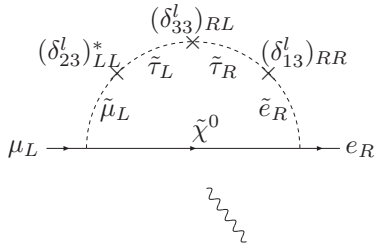

Figure 2: Neutralino loop contribution to $\mu \to e\gamma$ with triple mass insertions.

but also that $(\delta^d_{33})_{RL} \equiv m_b(A - \mu \tan\beta)/\widetilde{m}^2_{\tilde{d}}$ is generically present and therefore it should not be ignored. An $s \to d$ equivalent has been used in the study of ϵ'/ϵ_K [37].

Another example is B_s-$\overline{B_s}$ mixing. This process is affected by $(\delta^d_{23})_{RR}$ as well. However, the B_s-$\overline{B_s}$ mixing constraint on $(\delta^d_{23})_{RR}$ greatly depends on the size of $(\delta^d_{23})_{LL}$ [36], and therefore it matters what value of the LL insertion we choose when we are focusing on the RR mixing. Apart from the simple-minded choice of vanishing LL insertion, one option is to set $(\delta^d_{23})_{LL} = (\delta^d_{23})_{RR}$ [7], which may be expected from a left-right symmetry. Another well-motivated value of $(\delta^d_{23})_{LL}$ is the one generated by RG running from the scale where the boundary condition is given down to the sparticle mass scale [8]. This value is shown in a rather obscure form in (2.28b) and (2.21). It comes from the CKM mixing of quark Yukawa couplings and is expected even with universal soft supersymmetry breaking terms at M_*. It should be reasonable to expect at least this amount of LL insertion, even if one allows for general non-universal boundary condition, which is the case in this work.

In the framework of supersymmetric GUT, the story can be extended in a more interesting way. The aforementioned parameter $(\delta^d_{23})_{RR}$ is related to $(\delta^l_{23})_{LL}$ at the GUT scale, and it can lead to LFV. An obvious decay mode is $\tau \to \mu\gamma$ [13 – 16]. It can serve as another constraint on $(\delta^d_{23})_{RR}$, under the assumption of SU(5) grand unification. A less obvious mode is $\mu \to e\gamma$. Due to the GUT symmetry, the CKM mixing leads to an off-diagonal element of the scalar mass matrix of the entire **10** members, while they run from the reduced Planck scale down to the GUT scale. With the help of $(\delta^l_{13})_{RR}$ produced in this way, one can complete a diagram for $\mu \to e\gamma$ with triple mass insertions shown in figure 2. This diagram receives m_τ/m_μ enhancement relative to the usual chargino loop since it is proportional to $(\delta^l_{33})_{RL}$ [12, 20, 38, 39]. Therefore it can give a strong restriction

JHEP11(2008)051

on $(\delta^l_{23})_{LL}$ and thus on $(\delta^d_{23})_{RR}$.

The above examples illustrate how much a constraint on a given mass insertion parameter can be strengthened due to the presence of another insertion. Then, the question would be what the reasonable default value of a mass matrix element is, while a particular mass insertion is being scanned. In this work, we take the following scheme for choosing the default value of a soft supersymmetry breaking parameter: by default, the **10** soft scalar mass matrix elements are set to the RG-induced values from the top Yukawa coupling and the CKM mixing, and the off-diagonal components of $\overline{\mathbf{5}}$ mass matrix are set to zero; we ignore scalar trilinear couplings supposing that a loop graph arising from a nontrivial A-term does not accidently cancel the contributions considered later.

Using this scheme, we carry out a numerical analysis taking the following steps. From the Yukawa couplings and gauge couplings at the weak scale, those at the GUT scale are computed by solving the one-loop RG equations. In this process, neutrino Yukawa couplings are ignored. After reaching the GUT scale, we move to the basis of q, $\overline{u}$, $\overline{d}$, l, and $\overline{e}$ such that Y_d and Y_e are diagonal. We assume that U_L and U_R are identity matrices, and thus q, $\overline{d}$, l, $\overline{e}$ are identical to their uppercase counterparts in (2.13). In terms of the superpotential parameters, this corresponds to the case where h_2 in (2.3) is such that it reproduces the observed down-type quark and charged lepton masses, and is diagonal in the basis where Y_D is diagonal. Consequences of relaxing this assumption will be discussed in section 4.2. In this super-CKM basis of down-type quarks and charged leptons at the GUT scale, we set the soft mass matrix of squarks to the form,

$$m_q^2 = m_0^2 \begin{pmatrix} 1 & (\delta^d_{12})_{LL} & (\delta^d_{13})_{LL} \\ (\delta^d_{12})^*_{LL} & 1 & (\delta^d_{23})_{LL} \\ (\delta^d_{13})^*_{LL} & (\delta^d_{23})^*_{LL} & 1 \end{pmatrix}, \quad m_d^2 = m_0^2 \begin{pmatrix} 1 & 0 & (\delta^d_{13})_{RR} \\ 0 & 1 & (\delta^d_{23})_{RR} \\ (\delta^d_{13})^*_{RR} & (\delta^d_{23})^*_{RR} & 1 \end{pmatrix}, \quad (3.1)$$

and we determine the slepton soft masses using (2.16) neglecting the $\mathcal{O}(\xi)$ corrections. The other scalar masses including those of Higgses are universally put to m_0. The trilinear scalar couplings are set to zero. With these boundary conditions given at the GUT scale, the one-loop RG evolution of the lagrangian parameters is performed down to the weak scale. In order to fill out the mass matrices of scalars, charginos, and neutralinos, we determine μ from the electroweak symmetry breaking condition, choosing the positive sign. We have numerically checked that changing the sign of μ does not make a substantial difference. Then, we have all the sparticle mass matrices needed to calculate flavor and CP violation quantities. We do not use mass insertion approximation, but employ mass eigenvalues and mixing matrices, thereby taking account of multiple insertion graphs automatically. For a quark sector amplitude, we keep only gluino loops, and disregard parametrically suppressed corrections from neutralino, chargino, and charged Higgs exchanges.

Regarding patterns of the mass insertion parameters in (3.1), we consider the four cases displayed in table 1. A parameter indicated as 'free' is a variable to be scanned over, and the other three are fixed at the respective specified numbers, according to the policy outlined above. Those numbers have been obtained by solving the RG equations for the soft scalar mass matrices with universal boundary conditions at the reduced Planck scale down to the GUT scale in a supersymmetric SU(5) model with minimal field content [12]. In this proce-

Figure	$\lvert(\delta^d_{12})_{LL}\rvert$	$\lvert(\delta^d_{13})_{LL}\rvert$	$\lvert(\delta^d_{23})_{LL}\rvert$	$\lvert(\delta^d_{13})_{RR}\rvert$	$\lvert(\delta^d_{23})_{RR}\rvert$
4	4.8×10^{-5}	1.5×10^{-3}	7.4×10^{-3}	0	free
5	4.8×10^{-5}	1.5×10^{-3}	7.4×10^{-3}	free	0
6	4.8×10^{-5}	1.5×10^{-3}	free	0	0
7	4.8×10^{-5}	free	7.4×10^{-3}	0	0

Table 1: Values of mass insertion parameters to be given as boundary conditions at the GUT scale, for the case with $m_0 = 220$ GeV, $M_{1/2} = 180$ GeV, and $\tan\beta = 5$. The phase of a fixed $(\delta^d_{ij})_{LL}$ is equal to $\arg(-V^*_{ti}V_{tj})$, as can be expected from (2.21). The first column points to the plot of each free variable.

Observable	Measured value	Imposed constraint
ΔM_{B_d}	0.507 ± 0.004 ps^{-1} [23]	0.507 ps^{-1} $\pm$ 30%
$\sin 2\beta$	0.681 ± 0.025 [23]	2 σ
$\cos 2\beta$	> -0.4 [40]	
$B(B \to X_d\gamma)$	$(3.1 \pm 0.9^{+0.6}_{-0.5} \pm 0.5)\times10^{-6}$ [41]	$[5\times10^{-7}, 10^{-5}]$
ΔM_{B_s}	$17.77 \pm 0.10 \pm 0.07$ ps^{-1} [3]	17.77 ps^{-1} $\pm$ 30%
ϕ_{B_s}	$-0.57^{+0.24+0.07}_{-0.30-0.02}$ [6]	$[-1.20, 0.06]$
	$-0.76^{+0.37}_{-0.33}$, $-2.37^{+0.33}_{-0.37}$ [23]	$[-1.26, -0.13] \cup [-3.00, -1.88]$
$B(B \to X_s\gamma)$	$(352 \pm 23 \pm 9)\times10^{-6}$ [23]	2 σ
$S^{\phi K}_{\rm CP}$	0.39 ± 0.17 [23]	2 σ
$\lvert\epsilon_K\rvert$	$(2.232 \pm 0.007)\times10^{-3}$ [29]	$\lvert\epsilon_K^{\rm SUSY}\rvert < \lvert\epsilon_K^{\rm exp}\rvert$
ϵ'/ϵ_K	$(1.66 \pm 0.26)\times10^{-3}$ [29]	$\lvert(\epsilon'/\epsilon_K)^{\rm SUSY}\rvert < \lvert(\epsilon'/\epsilon_K)^{\rm exp}\rvert$
$\lvert d_n\rvert$	$< 6.3\times10^{-26}\ e\,$cm [42]	

Table 2: Constraints from the quark sector on sfermion mixing. An empty third column means that the second column is used as is.

dure, we have ignored effects of non-renormalizable operators on the running of scalar mass matrices. The size of $(\delta^d_{ij})_{LL}$ depends on m_0, $M_{1/2}$, and $\tan\beta$, where $M_{1/2}$ is the unified gaugino mass at $M_{\rm GUT}$. This dependence is taken into account in a plot for a different set of input parameters, although the change from the value shown in the table is insignificant.

3.2 Observables

We summarize observables from the quark sector and how we use them as constraints, in table 2.

The mass splittings of B^0 and B_s mesons have been measured with high precision. The error of ΔM_{B_d} is 0.8% and that of ΔM_{B_s} is 0.7%. However, their theoretical prediction from short-distance physics is not so precise. The main obstacle stems from $f^2_{B_d}B_{B_d}$ ($f^2_{B_s}B_{B_s}$) which enters the hadronic matrix element of B^0-$\overline{B^0}$ (B_s-$\overline{B_s}$) mixing, parametrizing long-distance QCD effects. The present uncertainty in lattice QCD calculation is around 30% (see e.g. [43] and references therein). A popular way to avoid this large uncertainty is to take the ratio $\Delta M_{B_s}/\Delta M_{B_d}$ since the error in $(f^2_{B_s}B_{B_s})/(f^2_{B_d}B_{B_d})$ is much smaller. Still,

JHEP11(2008)051

the SM prediction of the mass difference ratio has an uncertainty of about 40% due to the errors in the CKM matrix elements [43]. As a comprehensive way to embrace the above uncertainties, we require that each of computed ΔM_{B_d} and ΔM_{B_s} falls within 30% of its central value, fixing $f_{B_d}^2 B_{B_d}$ and $f_{B_s}^2 B_{B_s}$. In spite of the seemingly loose conditions, we will find that these requirements play impressive roles, given higher soft scalar mass. The uncertainty decreases with the progress of lattice QCD, and is estimated to be reducible down to 8–10% with 6–60 tera flops year of computing power [44]. The improved constraint from this smaller error is considered as well.

Although $\sin 2\beta$ does not suffer from uncertainty in the $\Delta B = 2$ matrix element, its SM prediction depends on V_{ub}, which has a sizable error. When we require $\sin 2\beta$ to be within the 2 σ range of its experimental value, we allow for a 2 σ variation in $|V_{ub}| = (4.31 \pm 0.30) \times 10^{-3}$ [29] as well. As with the magnitude of mixing, we estimate effects of an improved measurement of $\sin 2\beta$ at a super B factory, under the assumption that it will converge to its SM value. We use 2% as a projected error of $|V_{ub}|$ and 0.005 as a stadard deviation of $\sin 2\beta$ [45]. Given these smaller errors, the central values of $|V_{ub}|$ and $\sin 2\beta$, if they remain as they are now, become inconsistent with each other, reflecting the present tension between them. Under this condition, the future $\sin 2\beta$ measurement would appear to exclude the SM, and therefore it would be hard to evaluate the influence of its improved precision. However, there is a claim that the tension can be reconciled within the SM [46]. We do not regard this as a signal of new physics, and assume that $|V_{ub}|$ will decrease so that it becomes compatible with the present $\sin 2\beta$.

As for ϕ_{B_s}, the phase of B_s-$\overline{B_s}$ mixing, we try two distinct ways of imposing the constraint: (a) using the latest data from DØ at 90% confidence level (CL); (b) employing the 90% CL range recently reported by the Heavy Flavor Averaging Group (HFAG). Regarding option (b), we choose the one obtained with constraints from flavor-specific B_s lifetime and B_s semileptonic asymmetry. (What is denoted by ϕ_{B_s} in this work is $\phi_s^{J/\psi\phi}$ in the notation of HFAG.) We present both of these cases as they lead to very different impressions of the results—the DØ range includes the SM prediction of ϕ_{B_s} and hence it still works as a bound on the room for new physics, while the HFAG range lies outside the SM value, thereby indicating the size of extra contribution required to account for the discrepancy [47, 48]. In order to compare the power of ϕ_{B_s} measurements at LHCb with that of LFV, we suppose that the future central value of ϕ_{B_s} is given by the SM, despite the current hint of new physics at the level around 2 σ. We assume that the error of ϕ_{B_s} will be 0.009 at 10 fb^{-1} [49].

Measurement of the inclusive branching fraction $B(B \to X_d\gamma)$ had not been available until its preliminary result was recently reported from BaBar [41]. The precision is still low. Considering the experimental and theoretical uncertainties, we take modest upper and lower bounds guesstimated from the exclusive branching fraction $B(B \to \rho/\omega\,\gamma) = (1.18 \pm 0.17) \times 10^{-6}$ [23]. Unlike $B \to X_d\gamma$, the branching ratio of $B \to X_s\gamma$ has been measured with a high precision. We impose a 2 σ constraint on it.

We use QCD factorization [50] to evaluate $S_{\rm CP}^{\phi K}$, the sine term coefficient in the time-dependent CP asymmetry of $B \to \phi K$ [51, 52]. This approach has a source of hadronic uncertainty stemming from regularizing a divergent integral in the annihilation contri-

JHEP11(2008)051

Mode	Present bound	Future bound
$B(\mu \to e\gamma)$	1.2×10^{-11} [54]	10^{-13} [11]
$B(\tau \to e\gamma)$	1.1×10^{-7} [55]	10^{-8} [56], 2×10^{-9} [45]
$B(\tau \to \mu\gamma)$	4.5×10^{-8} [57]	10^{-8} [56], 2×10^{-9} [45]

Table 3: Constraints from radiative LFV decay modes.

Observable	Measured value
$S_{\rm CP}^{K^*\gamma}$	-0.19 ± 0.23 [23]
$S_{\rm CP}^{\rho\gamma}$	$-0.83 \pm 0.65 \pm 0.18$ [58]
$S_{\rm CP}^{B_s\to K^*\gamma}$	
$A_{\rm CP}^{b\to s\gamma}$	0.004 ± 0.037 [23]
$A_{\rm CP}^{b\to d\gamma}$	
$A_{\rm CP}^{b\to (s+d)\gamma}$	

Table 4: Monitored observables. Precisions attainable at a super B factory are summarized in table 6.

bution. We follow the original prescription in ref. [50], i.e. we replace $\int_0^1 dy/y$ by $X_A = (1+\varrho\, e^{i\varphi}) \ln(m_B/\Lambda_h)$, with $\Lambda_h = 500$ MeV, $0 \le \varrho \le 1$, and $0 \le \varphi < 2\pi$ [52]. We regard $S_{\rm CP}^{\phi K}$ as consistent with the data if it is less than 2 σ away from the central value for any ϱ and φ.

We also incorporate the CP violation parameters ϵ_K and ϵ'/ϵ_K in $K_L \to \pi\pi$ in the list. Although we do not explicitly scan over a 1-2 mixing, kaon physics can be influenced by double or higher order insertions. Imposing those constraints, we require that new physics contribution to each does not exceed the measured value in size. Concerning ϵ_K, its prediction from squark mixing can be made with an uncertainty much smaller than $|\epsilon_K^{\rm exp}|$. However, we are assuming that there may be an arbitrary 1-2 squark mixing, although we do not make a plot for it. This is why we are using a rather conservative bound.

Finally, we examine d_n the neutron electric dipole moment (EDM). Recently it has been pointed out that this observable can be greatly influenced if there are both LL and RR down-type squark mixings at the same time [53]. In order to evaluate d_n, we add contributions through the down quark EDM, down quark chromoelectric dipole moment (CEDM), and strange quark CEDM.

We use the constraints from the lepton sector listed in table 3. The second column shows the present 90% CL upper bound on each mode. The third column is the prospective upper bound from future experiments. The new limit on $\mu \to e\gamma$ is the goal of MEG at 90% CL. Also, higher sensitivity to $\tau \to e\gamma$ and $\tau \to \mu\gamma$ is anticipated from a super B factory. In section 4.1, we choose to use 10^{-8} as the future limit on $B(\tau \to e\gamma)$ and $B(\tau \to \mu\gamma)$, between the two numbers in each row of the table. If one wants to use 2×10^{-9} instead, the result can be obtained easily: multiply the upper bound on a given mass insertion from $\tau \to e\gamma$ or $\tau \to \mu\gamma$, by $1/\sqrt{5}$.

Imposing the conditions enumerated above, we estimate possible deviations in additional observables of interest, shown in table 4. The first three measure time-dependent

JHEP11(2008)051

CP asymmetries in radiative B decays. The definition of $S_{\rm CP}^{K^*\gamma}$ is given by [59],

$$\begin{aligned}\mathcal{A}_{K^*\gamma}(t) \equiv& \frac{\Gamma(\overline{B_d}(t)\to K^*\gamma)-\Gamma(B_d(t)\to K^*\gamma)}{\Gamma(\overline{B_d}(t)\to K^*\gamma)+\Gamma(B_d(t)\to K^*\gamma)}\\ =&A_{\rm CP}^{K^*\gamma}\cos(\Delta M_{B_d}t)+S_{\rm CP}^{K^*\gamma}\sin(\Delta M_{B_d}t).\end{aligned} \tag{3.2}$$

Note that the time-dependent CP asymmetry in $B_d\to K^*\gamma$ in our convention has the sign opposite to that in the above reference. This observable is sensitive to a new CP violating phase in the right-handed $b\to s$ transition, such as coming from $(\delta_{23}^d)_{RR}$. We define $S_{\rm CP}^{\rho\gamma}$ in a parallel way by replacing K^* with ρ in the expression. This can serve as a $b\to d$ analog of $S_{\rm CP}^{K^*\gamma}$, affected by $(\delta_{13}^d)_{RR}$. One might as well use $S_{\rm CP}^{B_s\to K^*\gamma}$ to investigate $(\delta_{13}^d)_{RR}$, and we record its variation. The rest three are direct CP asymmetries in radiative B decays, $B\to X_s\gamma$, $B\to X_d\gamma$, and $B\to X_{s+d}\gamma$, whose definitions can be figured out by setting $t=0$ in the above equation. They are complementary to the preceding observables in the sense that they can probe left-handed CP violating new physics such as $(\delta_{23}^d)_{LL}$ and $(\delta_{13}^d)_{LL}$. We quote the measured value of each observable if available.

4. Results

4.1 Viable region of each mass insertion

As a preparation for reading plots of the GUT scale mass insertions, we sketch the process amplitudes in terms of these variables. This will help us understand how a figure changes as a parameter is modified. Keeping only factors of interest, the LFV decay amplitudes can be roughly put in the form,

$$A(\tau\to\mu\gamma)\propto\frac{\mu\tan\beta\cdot(\delta_{23}^l)_{LL}(M_{\rm GUT})}{m_S^2}, \tag{4.1a}$$

$$A(\mu\to e\gamma)\propto\frac{m_\tau\mu\tan\beta}{m_0^2}\times\frac{(\delta_{13}^l)_{RR}(M_{\rm GUT})\cdot(\delta_{32}^l)_{LL}(M_{\rm GUT})}{m_S^2}, \tag{4.1b}$$

where m_S is the typical mass of a slepton, chargino, or neutralino in the loop. The first factor in the second line is $(\delta_{33}^l)_{RL}\equiv m_\tau(A-\mu\tan\beta)/\widetilde{m}_{\tilde{l}}^2$ rewritten with (2.25b). We used (2.30) to replace the other mass insertions by the GUT scale quantities. As to hadronic observables, let us pick up ΔM_{B_s} as an example; other constraints can be understood in a similar fashion. The B_s-$\overline{B_s}$ transition amplitude depends on $(\delta_{23}^d)_{AA}(\delta_{23}^d)_{BB}/m_S^2$ with $A,B=L,R$. For instance, we can use (2.28) to recast one of these combinations at $M_{\rm SUSY}$ as

$$\left.\frac{(\delta_{23}^d)_{LL}(\delta_{23}^d)_{RR}}{m_S^2}\right|_{M_{\rm SUSY}}\approx\frac{[(\delta_{23}^d)_{LL}(M_{\rm GUT})+q_{ij}]\cdot(\delta_{23}^d)_{RR}(M_{\rm GUT})}{(1+6x)^2m_S^2}, \tag{4.2}$$

where m_S is the typical mass of a squark or gluino in the loop. Note that q_{ij} from (2.29) is nearly independent of m_0^2. Therefore, as we vary m_0 and $M_{1/2}$, the scaling property of (4.2) is determined by its denominator. The other two combinations with $A=B=L,R$ scale in the same way.

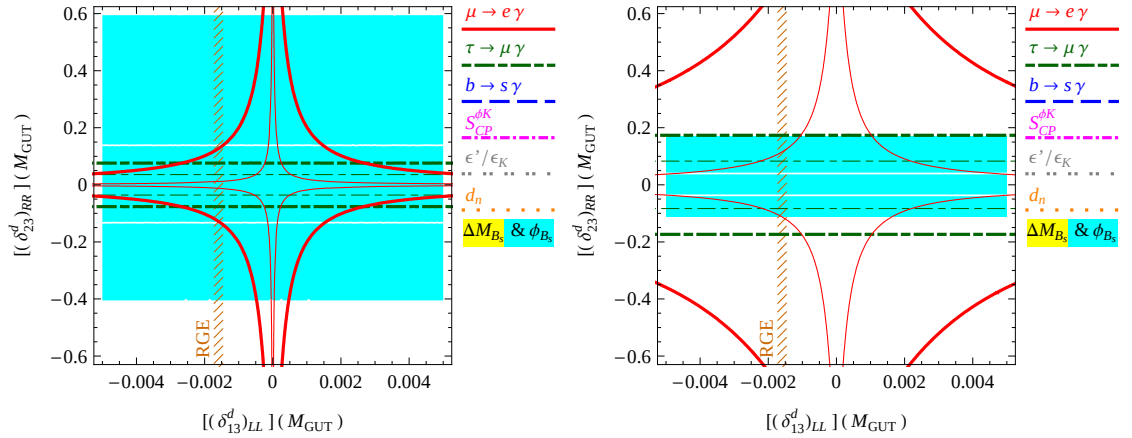

(a) $m_0 = 220$ GeV, $M_{1/2} = 180$ GeV, $\tan\beta = 5$ (b) $m_0 = 600$ GeV, $M_{1/2} = 180$ GeV, $\tan\beta = 5$

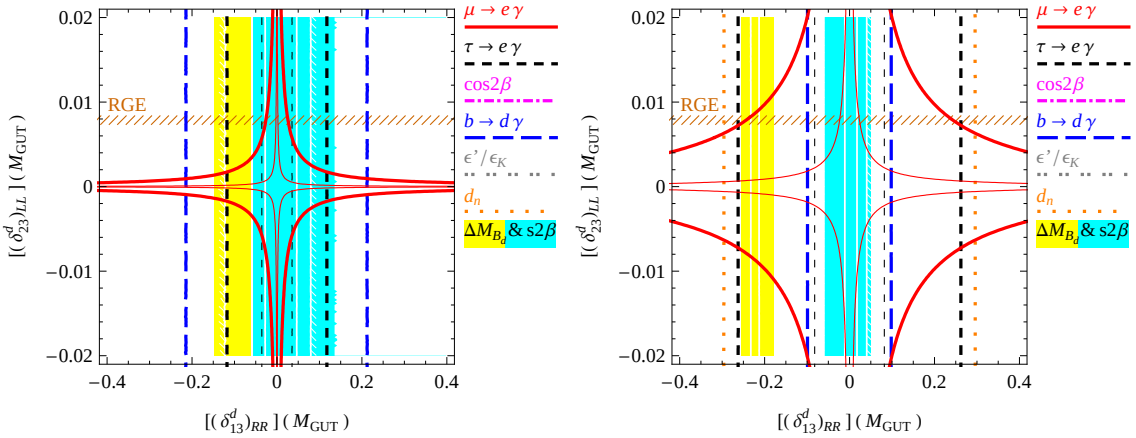

(c) $m_0 = 220$ GeV, $M_{1/2} = 180$ GeV, $\tan\beta = 5$ (d) $m_0 = 600$ GeV, $M_{1/2} = 180$ GeV, $\tan\beta = 5$

Figure 3: Constraints on [(a), (b)] the $((\delta^d_{13})_{LL}, (\delta^d_{23})_{RR})$ and [(c), (d)] the $((\delta^d_{13})_{RR}, (\delta^d_{23})_{LL})$ planes. For each LFV process, the thick curve is the present upper bound and the thin curve is the prospective future bound. A light gray (yellow) region is allowed by [(a), (b)] ΔM_{B_s} or [(c), (d)] ΔM_{B_d}, given 30% uncertainty in the $\Delta B = 2$ matrix element, and a gray (cyan) region is further consistent with [(a), (b)] ϕ_{B_s} from DØ or [(c), (d)] $\sin 2\beta$. The white lines around the center mark a possible improved constraint from [(a), (b)] ΔM_{B_s} or [(c), (d)] ΔM_{B_d}, with 8% hadronic uncertainty. The white curves with short thin lines attached to them display a measurement of [(a), (b)] ϕ_{B_s} at LHCb or [(c), (d)] $\sin 2\beta$ at a super B factory. Those short lines indicate the excluded side. Contributions from RG evolution to [(a), (b)] $(\delta^d_{13})_{LL}$ and [(c), (d)] $(\delta^d_{23})_{LL}$ are indicated by the vertical and the horizontal hatched strips, respectively. Their widths do not have any meaning.

With these ingredients at hand, we begin to interpret the results. First of all, let us look at the result of a two-parameter scan to get a taste of two mass insertions. In each of the four plots shown in figures 3, there are 1-3 and 2-3 mixings with different chiralities. The gaugino mass $M_{1/2}$ at the GUT scale is chosen in such a way that the gluino mass becomes 500 GeV at the weak scale. The scalar mass m_0 at $M_{\rm GUT}$ is set to two different

JHEP11(2008)051

values that can elucidate complementarity of the quark and the lepton sector processes. In the left column, m_0 is taken to be 220 GeV, so that the first and the second family right-handed down-type squarks have the same mass as the gluino at the weak scale. (The third family is slightly lighter.) This is a benchmark case often encountered in the literature on supersymmetric flavor violation. In the right column, we change m_0 to 600 GeV. If one fixes the δ parameters at $M_{\rm GUT}$, this m_0 maximizes gluino loop contribution to B-meson mixing for the gaugino mass chosen here. We elaborate on this point later. On the plots, each mass insertion parameter is treated as a real number.

In each of figures 3 (a) and (b), the two axes are $(\delta^d_{13})_{LL} = (\delta^l_{13})^*_{RR}$ and $(\delta^d_{23})_{RR} = (\delta^l_{23})^*_{LL}$ at the GUT scale. Here we restrict the horizontal axis to a range much narrower than the vertical axis since we are especially interested in the effect of RG contribution, but otherwise the LL mixing can be arbitrary. One can find that $(\delta^d_{23})_{RR}$ is constrained by $\tau \to \mu\gamma$ and ΔM_{B_s}. Interestingly, the two plots show different relative significance of these two constraints. In figure (a), $\tau \to \mu\gamma$ is stronger than ΔM_{B_s}, i.e. a large portion of the region allowed by the latter is excluded by the former. In figure (b), the order of importance appears to be reversed. Although it is early to draw a conclusion since these plots restrict the mass insertions to be real, it is obvious that ΔM_{B_s} gets tighter while $\tau \to \mu\gamma$ becomes looser if m_0 is changed from 220 GeV to 600 GeV. As m_0 increases, the LFV constraints get relaxed because m_S gets bigger in (4.1). In fact, μ in a numerator grows as well, but the growth of m_S^2 in the denominator wins. In spite of heavier sparticles, hadronic constraints get relatively more stringent. To understand why, pay attention to (4.2). Since we have fixed the gluino mass while raising m_0, a squark is heavier than a gluino, and we should substitute (2.25a) for m_S^2. Then, the gluino loop contribution to B_s-$\overline{B_s}$ mixing scales like $x/(1+6x)^3$. This factor increases as we decrease x inversely proportional to m_0^2, unless x is smaller than 1/12, the maximum point. For $x \lesssim 1/12$, the squarks are so heavy that they begin to decouple from low-energy processes as in split supersymmetry. Note that $x = 0.67$ on the left plot and $x = 0.09$ on the right. This explains the narrower ΔM_{B_s} band on the right plot.[1] Other quark sector processes are enhanced in a similar way, as will be shown later. As can be expected from figure 2, $\mu \to e\gamma$ restricts the product $(\delta^d_{13})_{LL}(\delta^d_{23})_{RR}$, resulting in the hyperbolas on the plane. Therefore, the $\mu \to e\gamma$ limit on $(\delta^d_{23})_{RR}$ varies depending on the size of $(\delta^d_{13})_{LL}$. If $(\delta^d_{13})_{LL} = 0$, $(\delta^d_{23})_{RR}$ is free, but the restraint grows severer as $|(\delta^d_{13})_{LL}|$ increases. A special case with RG-induced $(\delta^d_{13})_{LL}$, marked by the vertical hatched strip, will be detailed shortly. With increasing m_0, $\mu \to e\gamma$ is doubly suppressed by $m_0^2\, m_S^2$ in (4.1b). This expands the area within the hyperbola in the plots. The width of the ΔM_{B_s} band is mainly due to the current uncertainty in the B_s-$\overline{B_s}$ mixing matrix element around 30%. The projected bound with 8% uncertainty is depicted by the two white lines around $(\delta^d_{23})_{RR} = 0$. In figure (a), it is not yet as tight as the present $\tau \to \mu\gamma$ constraint which will be even tighter in the future. However, in figure (b), the reduced hadronic uncertainty makes the ΔM_{B_s} bound more restrictive than

[1] A similar discussion is given in ref. [34] in a different context, in a more qualitative way. In their scenario, the 2-3 squark mixing arises from large neutrino Yukawa couplings. They state that squark loop effects on B_s mixing can be more significant for higher m_0. However, they do not mention at what point of m_0 this trend stops and squark loops begin to decouple.

JHEP11(2008)051

$\tau \to \mu\gamma$ at a super B factory. Nevertheless, it should be kept in mind that $\tau \to \mu\gamma$ becomes more sensitive as tanβ grows while B_s-$\overline{B_s}$ mixing does not.

We do the same exercise with a different mixture of mass insertions, $(\delta^d_{13})_{RR} = (\delta^l_{13})^*_{LL}$ and $(\delta^d_{23})_{LL} = (\delta^l_{23})^*_{RR}$, to get figures 3 (c) and (d). The vertical range is set around the magnitude generated by RG running. Here $(\delta^d_{13})_{RR}$ is bounded by ΔM_{B_d}, $\sin 2\beta$, $\tau \to e\gamma$, and $B \to X_d\gamma$. In figure (c), the current limits from ΔM_{B_d} and $\tau \to e\gamma$ are comparable to each other, which are stronger than $B \to X_d\gamma$. In figure (d), ΔM_{B_d} with the aid of $\sin 2\beta$ leaves a band which is much narrower than that allowed by $\tau \to e\gamma$. Also, the $B \to X_d\gamma$ bound moves inside the $\tau \to e\gamma$ bound. These changes, as well as enhancement of the other quark sector processes, can be understood in the same way as the difference between figures (a) and (b). The inner two white lines around $(\delta^d_{13})_{RR} = 0$ indicate the limit from ΔM_{B_d} with 8% uncertainty in the B^0-$\overline{B^0}$ mixing matrix element, and the outer two white lines with short thin lines attached to them arise from $\sin 2\beta$ at a super B factory. The projected limits from ΔM_{B_d} and $\tau \to e\gamma$ are expected to maintain the present tendency of relative strengths. That is, they are comparable to each other in figure (c) and the former is stronger than the latter in figure (d). Again, the hyperbolas come from $\mu \to e\gamma$. Boundaries by the neutron EDM appear in figure (d) even though all the mixings are real. Extra contribution to d_n arises from the combination $(\delta^d_{13})_{LL}(\delta^d_{13})^*_{RR}$ of which the LL insertion picks up a non-vanishing phase from the CKM matrix, running from the GUT scale down to the weak scale. A specific case with RG-induced $(\delta^d_{23})_{LL}$, indicated by the horizontal hatched strip, will be discussed later.

Having grasped a picture of how different constraints act on two mass insertions, let us examine cases where one of the insertions originates from RG running from the reduced Planck scale to the GUT scale.

We display in figures 4, complex versions of figures 3 (a) and (b) with the LL insertions fixed at the numbers shown in table 1. They indicate regions of $(\delta^d_{23})_{RR} = (\delta^l_{23})^*_{LL}$ (in)consistent with observations. This time, tanβ is varied as well as m_0. Let us walk through them starting from figure 4 (a). A light gray (yellow) area is allowed by ΔM_{B_s} but not by ϕ_{B_s} from DØ. A gray (cyan) area is allowed by both. However, most of it is ruled out by the LFV processes, as we have already noticed in figure 3 (a). One can guess that this should be the case even in the near future, comparing the zone surrounded by the white curves and the thin circles with their centers at the origin. In particular, the $\mu \to e\gamma$ data from the MEG experiment should be able to kill all the parameter space except for the tiny disk around the origin. It deserves a remark that $\mu \to e\gamma$ is playing an important role here. Being a 2-3 mixing, $(\delta^d_{23})_{RR}$ is normally associated with the $\tau \to \mu\gamma$ process. For example, ref. [16] discusses interplay between leptonic and hadronic constraints in a similar context, but they use only $\tau \to \mu$ transitions to restrict $(\delta^d_{23})_{RR}$. This difference arises from the strategy of setting the mass insertion parameters. Their default value of a mass insertion is zero, while our default is the one which is minimally expected from RG running. Therefore, they do not find $\mu \to e\gamma$ limiting a 2-3 mixing as is obvious from figure 3 (a). We believe that our choice of mass insertions is more reasonable in a scenario where the soft terms are generated around the Planck scale such as gravity mediation. It may be argued that the RG-induced **10** scalar mixing is not always guaranteed to be

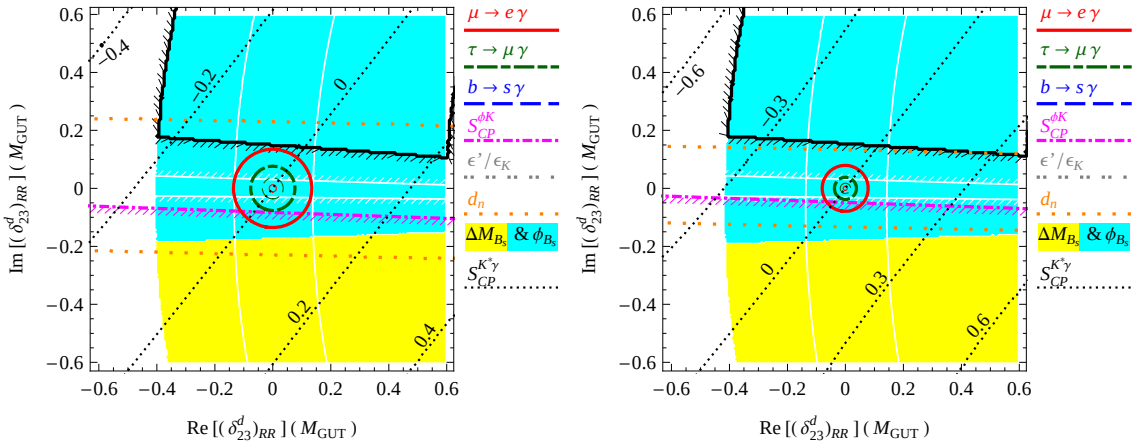

(a) $m_0 = 220$ GeV, $M_{1/2} = 180$ GeV, $\tan\beta = 5$ (b) $m_0 = 220$ GeV, $M_{1/2} = 180$ GeV, $\tan\beta = 10$

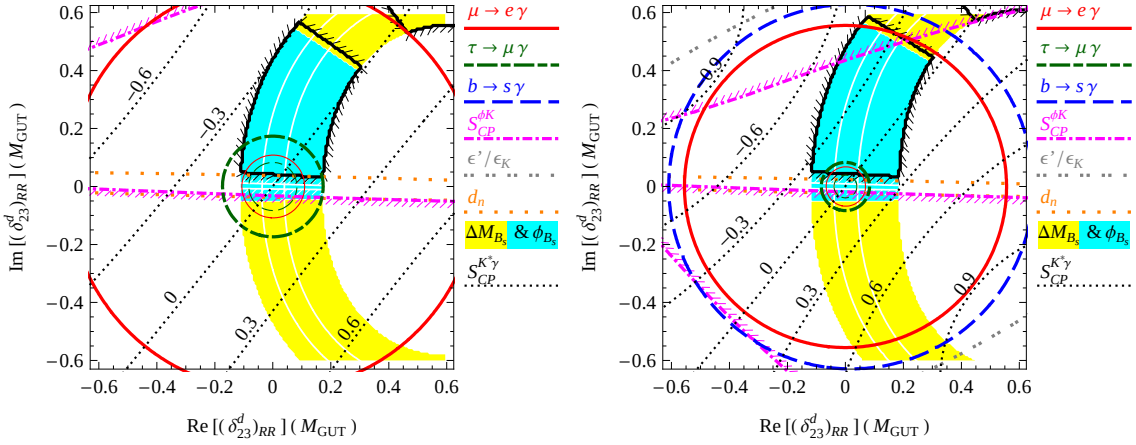

(c) $m_0 = 600$ GeV, $M_{1/2} = 180$ GeV, $\tan\beta = 5$ (d) $m_0 = 600$ GeV, $M_{1/2} = 180$ GeV, $\tan\beta = 10$

Figure 4: Constraints on the complex plane of $(\delta_{23}^d)_{RR}$, with $(\delta_{ij}^d)_{LL}$ generated from RG running between the reduced Planck scale and the GUT scale. For each LFV process, the thick circle is the present upper bound and the thin circle is the prospective future bound. A light gray (yellow) region is allowed by ΔM_{B_s}, given 30% uncertainty in the $\Delta B = 2$ matrix element, and a gray (cyan) region is further consistent with ϕ_{B_s} from DØ. A thick black curve shows ϕ_{B_s} from HFAG. The white curves running from top to bottom mark a possible improved constraint from ΔM_{B_s} with 8% hadronic uncertainty. The other white lines running from left to right display a measurement of ϕ_{B_s} at LHCb. Thin short lines attached to a curve indicate the excluded side.

sizeable since the cutoff scale can happen to be low close to the GUT scale. This is true. However, a low cutoff would threaten the validity of making a connection between the quark and the lepton flavors in the first place. Non-renormalizable operators shown in (2.3) and even higher order terms, generically, give $\mathcal{O}(1)$ contributions to the quark and the lepton Yukawa couplings, thereby erasing any trace of their connection in the flavor space as a single GUT multiplet. It should be remembered that an RG-induced LL insertion is not

JHEP11(2008)051

only critical to $\mu \to e\gamma$, but also to B_s-$\overline{B_s}$ mixing. Indeed, the presence of $(\delta^d_{23})_{LL}$ is rendering the ΔM_{B_s} constraint on $(\delta^d_{23})_{RR}$ tighter [7, 8, 36]. If it were not for $(\delta^d_{23})_{LL}$, the gray region would look like the one in figure 6 (a), where the contribution to ΔM_{B_s} from $(\delta^d_{23})_{LL}$ is not enhanced by $(\delta^d_{23})_{RR}$. Another noticeable point is that the information on ϕ_{B_s} from LHCb can play an important role in shaping the allowed region. A particular pleasure with this constraint that it does not suffer from the hadronic uncertainty that plagues ΔM_{B_s}. Other observables of interest related to 2-3 mixing are $S^{\phi K}_{\rm CP}$ and d_n. The area excluded by each of them is depicted. Note that d_n depends on the phase of $(\delta^d_{23})_{LL}$ as well as on its size. Although the phase of the first term in (2.21) is fixed by the CKM matrix elements, the $\mathcal{O}(\xi)$ correction is unknown and may influence the phase of the entire insertion. Varying the phase of $(\delta^d_{23})_{LL}$ amounts to rotating the d_n band on the plot around the origin. Finally, the dotted lines are contours of $S^{K^*\gamma}_{\rm CP}$. From them, one can read off its largest possible deviation that is consistent with the other experimental inputs. Further information on this CP asymmetry is collected in section 4.4.

Now that we have recognized the general structure of a plot, we try different values of parameters. First, $\tan\beta$ is doubled from 5 to 10 in figure 4 (b). The ΔM_{B_s} belt does not change very much since its dependence on $\tan\beta$ is negligible. Each LFV circle halves and becomes tighter. This is evident from (4.1), where each decay amplitude is proportional to $\tan\beta$. The gluino loop diagrams contributing to each of d_n and the $B \to \phi K$ decay are also proportional to $\tan\beta$, and the allowed region shrinks as $\tan\beta$ increases. Next, we change the scalar mass parameter. In figure 4 (c), we raise m_0 to 600 GeV, a value optimized for B-meson mixings. For the reason already explained, the LFV constraints turn weaker while the B_s-$\overline{B_s}$ mixing belt shrinks on the plot. Other quark sector processes are boosted as well. Because of this, the impressions of hadronic and leptonic bounds undergo a sea change from figure (a) to (c). The current $\mu \to e\gamma$ limit gets so much relaxed that it does not exclude any region compatible with ΔM_{B_s} and ϕ_{B_s}. One can also notice that d_n has become much more powerful. Its limit on the imaginary part of $(\delta^d_{23})_{RR}$ is stronger than any other bound on the plot. Indeed, the combination of d_n and B_s-$\overline{B_s}$ mixing leaves nothing to do for $\tau \to \mu\gamma$. In the future case, B_s-$\overline{B_s}$ mixing looks more restrictive than $\tau \to \mu\gamma$ and $\mu \to e\gamma$, particularly thanks to improved precision of ϕ_{B_s} at LHCb. This should be contrasted with the situation in figure (a) where the LFV constraints, both at present and in the future, are stronger than the hadronic ones. Lastly, we consider higher m_0 and $\tan\beta$ in figure (d). Each observable changes according to its $\tan\beta$ dependence already mentioned. For the first time, the $B \to X_s\gamma$ bound becomes visible. Until now, its branching fraction has not been sufficiently disturbed by the new physics contribution given by figure 1 (b). One reason is that this diagram does not interfere with the SM one since they lead to different photon helicities. In figure 4 (d), however, higher m_0 and $\tan\beta$ cooperate to enhance the supersymmetric amplitude. Still, $B \to X_s\gamma$ is not very restrictive. Its role should be more significant for $\tan\beta$ much higher than 10. The range of $S^{K^*\gamma}_{\rm CP}$ predicted in each case is summarized in table 6.

A remark is in order regarding the recent reports on ϕ_{B_s} which reveal a small but interesting disparity between the combined fit and the SM prediction [22, 23]. Once we take the 90% CL range of ϕ_{B_s} from HFAG, instead of that from DØ, the gray regions

JHEP11(2008)051

change to those surrounded by the thick black curves. Since the HFAG result demands new physics contribution to ϕ_{B_s}, the origin on the plane is positioned outside the thick black boundary. On the other hand, the mass insertion can be compatible with the LFV data only around the origin. This conflict leads to a restriction in an attempt to understand the new fit result of ϕ_{B_s} with an RR mixing. The trouble is more serious with lower m_0 and/or higher $\tan\beta$. As was explained above, lower m_0 enhances the LFV branching ratios while suppressing supersymmetric contributions to B_s-$\overline{B_s}$ mixing. Also, higher $\tan\beta$ gives rise to higher LFV rates. Figures (a) and (b) tell us that these cases are disfavored by LFV in combination with ϕ_{B_s}. The tension between LFV and ϕ_{B_s} is relaxed for higher m_0 used in the lower plots. Indeed, one can find a small intersection of the ϕ_{B_s} area and the $\tau \to \mu\gamma$ disk in each of figures (c) and (d). This region could be accessed by measurements of $\tau \to \mu\gamma$ and $\mu \to e\gamma$ in the near future. However, the neutron EDM becomes a new obstacle to the zone favored by ϕ_{B_s} as higher m_0 reinforces hadronic constraints. The limit from d_n grows more serious for higher $\tan\beta$. The problem can be eased by modifying the size and phase of $(\delta^d_{23})_{LL}$ at the GUT scale to rotate the d_n band as already mentioned.

At this point we stop considering 2-3 mixing of $\overline{F}$, and apply the same procedure to the 1-3 sector. We present in figures 5, complex versions of figures 3 (c) and (d) with the LL insertions fixed at the values listed in table 1. They exhibit constraints on $(\delta^d_{13})_{RR} = (\delta^l_{13})^*_{LL}$. We start over with figure 5 (a). The light gray (yellow) belt is compatible with ΔM_{B_d}, which is further reduced by $\sin 2\beta$ into the gray (cyan) region. The resulting area is completely consistent with $B \to X_d\gamma$. The width of this area is comparable to the diameter of the circle from $\tau \to e\gamma$. The restriction from $\mu \to e\gamma$ is so strong that it rules out most of the gray zone. The $\mu \to e\gamma$ disk in this plot is smaller than that in figure 4 (a). The reason is that the decay amplitude is proportional to $(\delta^l_{23})_{RR} \sim \lambda^2$ here, but to $(\delta^l_{13})_{RR} \sim \lambda^3$ there. In a few years, improved lattice QCD should be able to narrow the ΔM_{B_d} belt down to the one between the two white curves, whose width is again comparable to the diameter of the future $\tau \to e\gamma$ disk. If this narrowed belt is complemented by measurement of $\sin 2\beta$ at a super B factory, the combined constraint could be comparable to or stronger than the future $\tau \to e\gamma$ bound. The MEG constraint is so tight that the circle appears to be a single dot at the origin. The radius of this circle can be looked up in table 5. The dotted curves are contours of $S^{\rho\gamma}_{\rm CP}$. We present its shift that can be expected obeying other constraints in section 4.4. The rest three plots are for the cases with (b) higher $\tan\beta$, (c) higher m_0, and (d) higher m_0 and $\tan\beta$, respectively. They can be understood in the same way as each corresponding figure in figures 4 was. Let us stress again that with higher m_0, the sensitivity of hadronic observables to the GUT scale mass insertions is reinforced while that of LFV is weakened. In figures (c) and (d), the combination of ΔM_{B_d} and $\sin 2\beta$ essentially determines the viable areas. This trend is expected to be maintained by a super B factory. One can notice that d_n in figures (c) and (d), and ϵ'/ϵ_K in figure (d), begin to be visible due to increased m_0. These quantities are susceptible to the imaginary parts of $(\delta^d_{13})_{RR}(\delta^d_{33})_{RL}(\delta^d_{31})_{LL}$ and $(\delta^d_{13})_{RR}(\delta^d_{33})_{RL}(\delta^d_{32})_{LL}$, respectively, although they are not playing important roles here. Figures 5 (b) and (d) show that the amplitude of $B \to X_d\gamma$ is enhanced by higher $\tan\beta$. One can see the reason replacing s by d in figure 1 (b).

JHEP11(2008)051

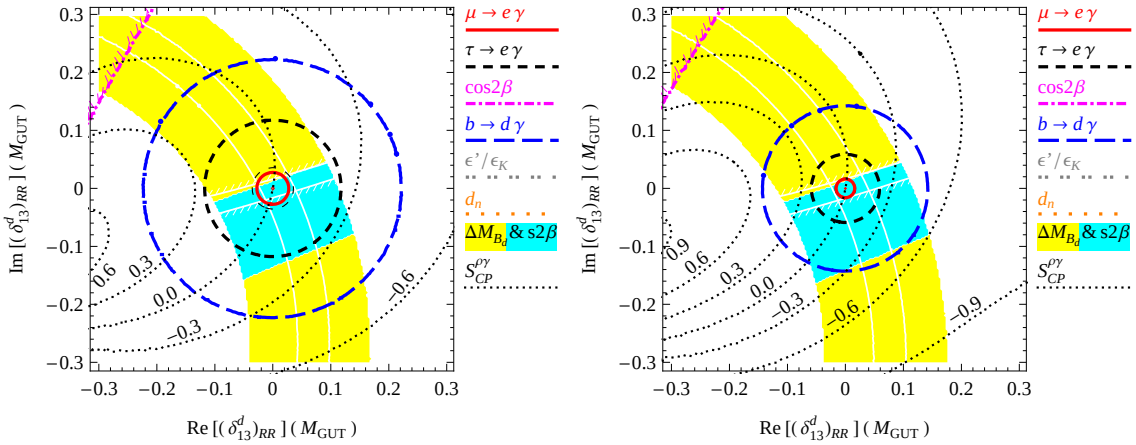

(a) $m_0 = 220$ GeV, $M_{1/2} = 180$ GeV, $\tan\beta = 5$ (b) $m_0 = 220$ GeV, $M_{1/2} = 180$ GeV, $\tan\beta = 10$

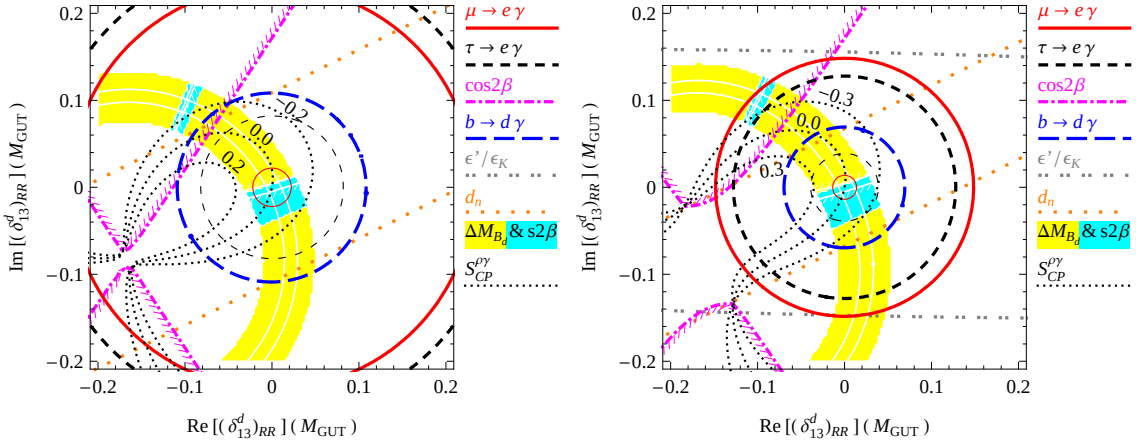

(c) $m_0 = 600$ GeV, $M_{1/2} = 180$ GeV, $\tan\beta = 5$ (d) $m_0 = 600$ GeV, $M_{1/2} = 180$ GeV, $\tan\beta = 10$

Figure 5: Constraints on the complex plane of $(\delta^d_{13})_{RR}$, with $(\delta^d_{ij})_{LL}$ generated from RG running between the reduced Planck scale and the GUT scale. For each LFV process, the thick circle is the present upper bound and the thin circle is the prospective future bound. A light gray (yellow) region is allowed by ΔM_{B_d}, given 30% uncertainty in the $\Delta B = 2$ matrix element, and a gray (cyan) region is further consistent with $\sin 2\beta$. The white curves running along the belt mark a possible improved constraint from ΔM_{B_d} with 8% hadronic uncertainty. The other white lines running across the belt display a measurement of $\sin 2\beta$ at a super B factory. Of the two sides of a $\cos 2\beta$ curve or a white $\sin 2\beta$ curve, the excluded one is indicated by thin short lines.

For the sake of completeness, we report restrictions on the **10** sector mixings as well, which can be represented by $(\delta^d_{ij})_{LL} = (\delta^l_{ij})^*_{RR}$. In figures 6, we examine the 2-3 mixing. Comparing them with figures 4, one can notice that B_s-$\overline{B_s}$ mixing is not as restrictive on $(\delta^d_{23})_{LL}$ as $(\delta^d_{23})_{RR}$. There, the gluino loop contribution from $(\delta^d_{23})_{RR}$ to the $\Delta B = 2$ transition was enhanced by $(\delta^d_{23})_{LL}$ from radiative correction. By contrast, $(\delta^d_{23})_{LL}$ here is not reinforced by $(\delta^d_{23})_{RR}$ which is set to zero. Nonetheless, ΔM_{B_s} and ϕ_{B_s} exclude part of

JHEP11(2008)051

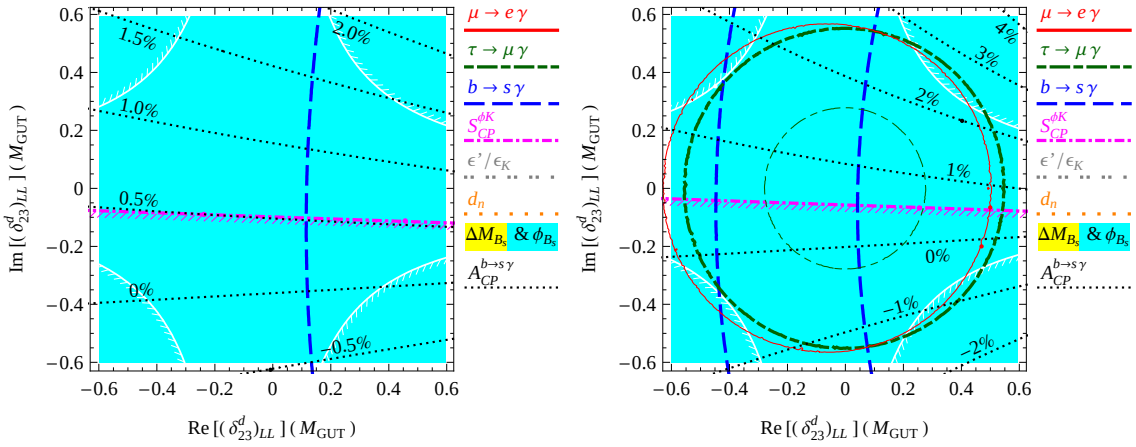

(a) $m_0 = 220$ GeV, $M_{1/2} = 180$ GeV, $\tan\beta = 5$ (b) $m_0 = 220$ GeV, $M_{1/2} = 180$ GeV, $\tan\beta = 10$

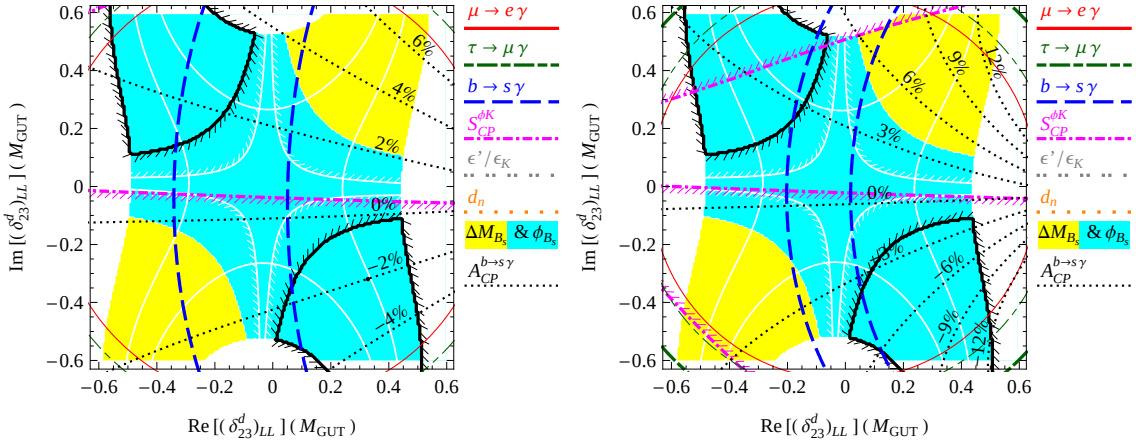

(c) $m_0 = 600$ GeV, $M_{1/2} = 180$ GeV, $\tan\beta = 5$ (d) $m_0 = 600$ GeV, $M_{1/2} = 180$ GeV, $\tan\beta = 10$

Figure 6: Constraints on the complex plane of $(\delta^d_{23})_{LL}$, with $(\delta^d_{12})_{LL}$ and $(\delta^d_{13})_{LL}$ generated from RG running between the reduced Planck scale and the GUT scale. For each LFV process, the thick circle is the present upper bound and the thin circle is the prospective future bound. A light gray (yellow) region is allowed by ΔM_{B_s}, given 30% uncertainty in the $\Delta B = 2$ matrix element, and a gray (cyan) region is further consistent with ϕ_{B_s} from DØ. A thick black curve shows ϕ_{B_s} from HFAG. The white curves without short thin lines mark a possible improved constraint from ΔM_{B_d} with 8% hadronic uncertainty. The white curves with short thin lines attached to them display a measurement of ϕ_{B_s} at LHCb. Thin short lines attached to a curve indicate the excluded side.

the plane in figures 6 (c) and (d) where their sensitivities to the GUT scale squark mixing are maximized. These constraints should be strengthened in the future. The white curves with short thin lines attached to them mark an improved ϕ_{B_s} measurement at LHCb. They appear in all the four cases. The other white curves, appearing in figures (c) and (d), represent the projected ΔM_{B_s} limit. Another outstanding point is that $B \to X_s\gamma$ is excluding larger area of the $(\delta^d_{23})_{LL}$ plane than $(\delta^d_{23})_{RR}$. Recall that the supersymmetric

JHEP11(2008)051

diagram arising from an LL mixing is added to the SM piece since they have the same chirality structure, while they do not interfere in the RR insertion case in figures 4. This bound grows more stringent for higher $\tan\beta$ as is evident from plots in the right column. The LFV constraints are noticeably weaker here than in figures 4. Concerning $\tau \to \mu\gamma$, this is because the decay is dominated by neutralino loop here, but by chargino loop there. The chargino loop, if present, generically has higher effectiveness per mass insertion size, than the neutralino loop. One can find that $\mu \to e\gamma$ also occurs. It is caused by a neutralino loop graph proportional to $(\delta^l_{23})_{RR}(\delta^l_{31})_{RR}$ with RG-induced $(\delta^l_{31})_{RR}$. However, it is not strengthened by the factor m_τ/m_μ, which accounts for the lower branching ratio than in figures 4. Despite being moderate, the present and future LFV bounds are still disallowing portions of the parameter space. The dotted contours show $A_{\rm CP}^{b\to s\gamma}$, the direct CP asymmetry in $B \to X_s\gamma$. The numerical value of its variation is shown in table 4, together with that of another related CP asymmetry, $A_{\rm CP}^{b\to(s+d)\gamma}$.

Now, we switch to the HFAG fit of the phase of B_s-$\overline{B_s}$ mixing. In figures 4 (a) and (b), we cannot find a point which falls within the 90% CL range of ϕ_{B_s}, even if we allow for an $\mathcal{O}(1)$ squark mixing. Favored regions appear in figures (c) and (d), where hadronic processes are enhanced. As those regions involve a large 2-3 mixing of left handed down-type squarks, they are likely to give a large modification to $B \to X_s\gamma$, in particular for high $\tan\beta$. In figure (d), one can notice that a substantial part of the zone of $(\delta^d_{23})_{LL}$, needed to fit ϕ_{B_s}, may conflict with $S_{\rm CP}^{\phi K}$. This conflict also grows more serious with increasing $\tan\beta$. In an attempt to account for the negative value of ϕ_{B_s} with an LL mixing, one could have a bigger hope, given a large mixing, higher m_0, and low $\tan\beta$. Even if this scenario is realized, $\tau \to \mu\gamma$ and $\mu \to e\gamma$ will be hard to observe even at a super B factory or MEG.

Finally, we proceed to the exclusion plots on the complex plane of $(\delta^d_{13})_{LL} = (\delta^l_{13})^*_{RR}$ in figures 7. Let us compare these with those in figures 5. A gray (cyan) region here is larger. A significant portion of a gray zone is cut out by $B \to X_d\gamma$ [60]. The LFV circles are significantly bigger. Each of the above facts can be explained in a parallel fashion as we did in the previous paragraph. The dotted contours are values of $A_{\rm CP}^{b\to d\gamma}$. Its discussion will follow in a later part. Note that there are cases where the future LFV data may kill part of the area that is compatible with B physics measurements. An example is shown in figure 7 (b) with lower m_0 and higher $\tan\beta$. Yet, constraints mostly come from the hadronic sector.

We finish this subsection with a remark on the sizes of the allowed regions shown in the preceding figures. We use mass insertion parameters at the GUT scale as the horizontal and vertical axes. Therefore, one should be careful in comparing a plot in this paper with one from another work, when the latter is using mass insertions at the weak scale. If the weak scale variable is a squark mass insertion, one should convert our plots using (2.28) beforehand.

4.2 Non-renormalizable operators and leptonic constraints

In the numerical analysis of the previous subsection, we have been employing the naive relations (2.18). Now, we should discuss how the results will change if we relax this simplification and generalize the correlation of mass insertions to (2.17). One could easily guess that the one-to-one correspondence between a hadronic and a leptonic channel should be

JHEP11(2008)051

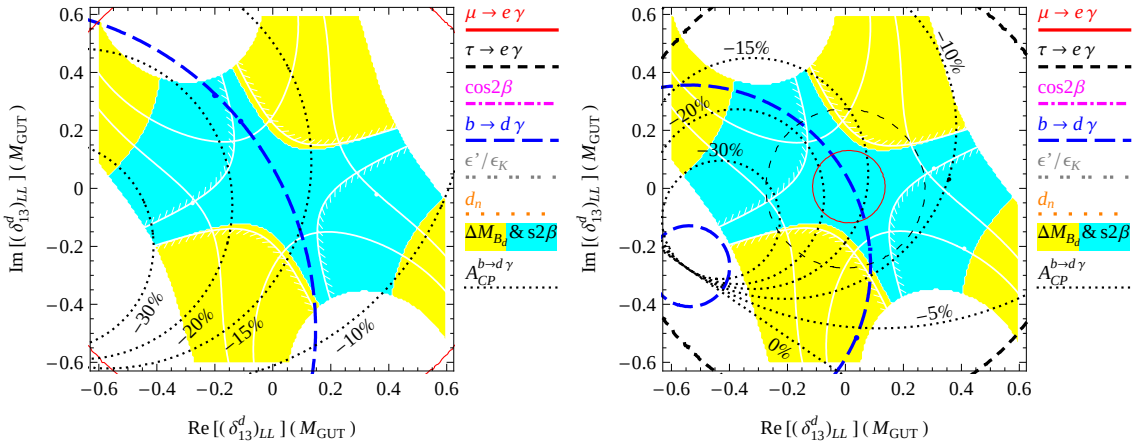

(a) $m_0 = 220$ GeV, $M_{1/2} = 180$ GeV, $\tan\beta = 5$ (b) $m_0 = 220$ GeV, $M_{1/2} = 180$ GeV, $\tan\beta = 10$

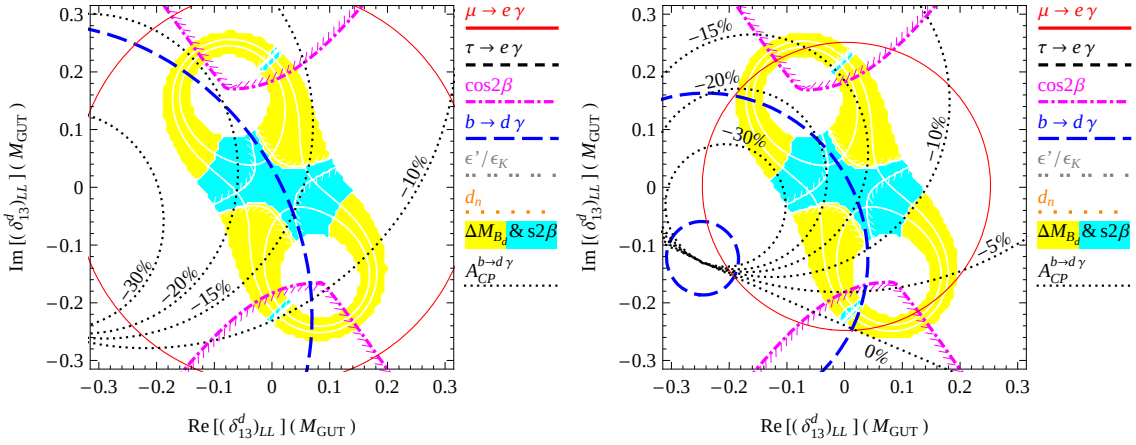

(c) $m_0 = 600$ GeV, $M_{1/2} = 180$ GeV, $\tan\beta = 5$ (d) $m_0 = 600$ GeV, $M_{1/2} = 180$ GeV, $\tan\beta = 10$

Figure 7: Constraints on the complex plane of $(\delta^d_{13})_{LL}$, with $(\delta^d_{12})_{LL}$ and $(\delta^d_{23})_{LL}$ generated from RG running between the reduced Planck scale and the GUT scale. For each LFV process, the thick circle is the present upper bound and the thin circle is the prospective future bound. A light gray (yellow) region is allowed by ΔM_{B_d}, given 30% uncertainty in the $\Delta B = 2$ matrix element, and a gray (cyan) region is further consistent with $\sin 2\beta$. The white curves without short thin lines attached to them mark a possible improved constraint from ΔM_{B_d} with 8% hadronic uncertainty. The white curves with short thin lines attached to them display a measurement of $\sin 2\beta$ at a super B factory. Of the two sides of a $\cos 2\beta$ curve or a white $\sin 2\beta$ curve, the excluded one is indicated by the thin short lines.

disturbed. Yet, it is not completely broken as will be shown below. Tau decay modes still limit 1-3 and 2-3 mixings of squarks of either chirality, albeit to a reduced extent. Similarly, $\mu \to e\gamma$ remains a constraint on the RR insertions.

Let us think about how a tau decay bound should be modified. We first focus on RR insertions, and then on LL. If there is an RR mixing, a tau decay amplitude is dominated

JHEP11(2008)051

by the chargino loop which is proportional to $(\delta^l_{13})_{LL}$ for $\tau \to e\gamma$ or $(\delta^l_{23})_{LL}$ for $\tau \to \mu\gamma$. Neglecting the $\mathcal{O}(\xi)$ term in (2.17a), one has

$$(\delta^l_{a3})_{LL} = [U_L]_{ab}\,(\delta^d_{b3})^*_{RR}\,[U_L]^*_{33} + \mathcal{O}(\cos^2\beta\,\delta^d_{RR}), \quad a, b = 1, 2, \tag{4.3}$$

using (2.12), the smallness of mixing of the third family with the other two. [By the same token as for (2.23), there can be another term $[U_L]_{a3}\,(\delta^d_{33})_{RR}\,[U_L]^*_{33} \sim 1.5 \times 10^{-5}/\cos\beta + 0.17\,\lambda_N^2\cos\beta$ where we use the $(3,3)$ component of (2.20b) for its estimation. For small neutrino Yukawa couplings, which we assume in the numerical analysis, this term is negligible even compared to the smallest upper bound that can be found in table 5. For large λ_N, this should be an uncertainty in relating squark and slepton mixings, apart from that stemming from running below $M_{\rm GUT}$.] The mixing between the first and the second families, parametrized by $[U_L]_{ab}$, is not limited to be small. For instance, consider the case where $(\delta^d_{23})_{RR}$ is nonzero while $(\delta^d_{13})_{RR}$ is zero, as in figures 4. Here, $\tau \to \mu\gamma$ provides a significant constraint on $(\delta^d_{23})_{RR}$ if U_L is a unit matrix. Otherwise, it might happen that the association of $(\delta^l_{23})_{LL}$ with $(\delta^d_{23})_{RR}$ is weakened by the factor $[U_L]_{22}$, or in the worst case, is completely broken for $[U_L]_{22} = 0$. Although $\tau \to \mu\gamma$ does not occur in this extreme situation, $\tau \to e\gamma$ does since $(\delta^d_{23})_{RR}$ gives rise to it through $(\delta^l_{13})_{LL}$ due to the approximate unitarity of $[U_L]_{ab}$. This argument, for a general $[U_L]_{ab}$, can be summarized in the form,

$$|(\delta^l_{13})_{LL}|^2 + |(\delta^l_{23})_{LL}|^2 \approx |(\delta^d_{13})_{RR}|^2 + |(\delta^d_{23})_{RR}|^2 + \mathcal{O}[\cos^2\beta\,(\delta^d_{RR})^2], \tag{4.4}$$

which determines $B(\tau \to (e+\mu)\,\gamma)$. The mass insertions appearing above are all at the GUT scale. Note that the current experimental bounds on $B(\tau \to \mu\gamma)$ and $B(\tau \to e\gamma)$ differ only by a factor of 2.4. Therefore, once one combines these two, one can always give an upper bound on each of $(\delta^d_{23})_{RR}$ and $(\delta^d_{13})_{RR}$, almost independent of U_L. The error caused by non-vanishing 1-3 or 2-3 mixing in U_L, is diminished below 10% even for $\tan\beta$ as low as 3. If one wants to apply this conservative constraint to the case of figures 4, the radius of each thick $\tau \to \mu\gamma$ circle should be enlarged by a factor of 1.9. The thick $\tau \to e\gamma$ circles in figures 5 should be expanded by a factor of 1.2. Similarly, the future bounds can be modified: multiply each by $\sqrt{2}$. Even in this case, tau decays remain severe constraints on sfermion mixings.

The same prescription can be applied to the tau decay bound on an LL mixing. Except that the amplitude is dominated by a neutralino loop, we can repeat the above line of reasoning with L and R exchanged. In this case, a possible additional term in (2.23) arising from $(\delta^d_{33})_{LL}$, discussed in section 2.2, is negligible relative to an upper limit from $\tau \to \mu\gamma$ or $\tau \to e\gamma$ shown in figures 6 and 7. One can obtain a region permitted by $\tau \to (e+\mu)\,\gamma$ in figures 6, multiplying the radius of a thick $\tau \to \mu\gamma$ circle by 1.9. The expansion factor for figures 7 is 1.2. Again, each future bound should be multiplied by $\sqrt{2}$.

Unlike the tau decay modes, $\mu \to e\gamma$ is more involved, and the following method is applicable only to an RR insertion. The dominant contribution comes from the triple insertion graph in figure 2. Including the diagram with opposite chirality structure, we find that the decay rate is proportional to

$$d \equiv |(\delta^l_{13})_{RR}(\delta^l_{32})_{LL}|^2 + |(\delta^l_{13})_{LL}(\delta^l_{32})_{RR}|^2. \tag{4.5}$$

JHEP11(2008)051

The $\mu \to e\gamma$ data supplies an upper limit on this quantity. One can use (4.4) to show that

$$d \gtrsim \min\{|(\delta^l_{13})_{RR}|^2, |(\delta^l_{23})_{RR}|^2\} \cdot [|(\delta^d_{13})_{RR}|^2 + |(\delta^d_{23})_{RR}|^2], \tag{4.6}$$

ignoring the term suppressed by $\cos^2\beta$. In contrast to $\tau \to (e+\mu)\,\gamma$, $\mu \to e\gamma$ depends on the new pivotal factors, $(\delta^l_{13})_{RR}$ and $(\delta^l_{23})_{RR}$. Ignoring the non-renormalizable operators, we had their values equal to those of $(\delta^d_{13})^*_{LL}$ and $(\delta^d_{23})^*_{LL}$ in table 1, respectively. As to how $(\delta^l_{13})_{RR}$ and $(\delta^l_{23})_{RR}$ change after the non-renormalizable operators are turned on, there are three logical possibilities: (a) each value remains at the same order of magnitude; (b) either is very small and the other is not; (c) both are vanishingly small. In Case (a), one can use (4.6) in order to translate the upper limit on d to those on $(\delta^d_{13})_{RR}$ and $(\delta^d_{23})_{RR}$, nearly independent of U_L. We have seen that both $(\delta^l_{13})_{RR}$ and $(\delta^l_{23})_{RR}$ are at least of the same order as $(\delta^d_{13})_{LL}$ from (2.24)—otherwise, they should belong to Case (b) or (c). Thus, the U_L-independent upper bound on each of $(\delta^d_{13})_{RR}$ and $(\delta^d_{23})_{RR}$, should be given by a $\mu \to e\gamma$ ring in figures 4. That is, figures 4 are not modified even with this conservative interpretation, while the $\mu \to e\gamma$ circles in figures 5 should be replaced by those in figures 4. In Case (b), the bound inevitably depends on U_L. As above, consider the scenario where $(\delta^d_{23})_{RR}$ is non-vanishing while $(\delta^d_{13})_{RR}$ vanishes. In addition, suppose that $(\delta^l_{23})_{RR}$, for example, happens to be highly suppressed. Then, (4.3) and (4.5) lead to

$$d \approx |(\delta^l_{13})_{RR}|^2 |(\delta^d_{23})_{RR}|^2 |[U_L]_{22}|^2. \tag{4.7}$$

The branching ratio scales like $|[U_L]_{22}|^2$. Therefore, a $\mu \to e\gamma$ circle in figure 4 should be enlarged by the factor $1/|[U_L]_{22}|$. However, we have learned in section 2.2 that Case (b) is not realized unless the mixing angle in $[U_R]_{ab}$ is fine-tuned. In Case (c), which requires a conspiracy of λ_U, λ_D, h_1, h_2, f_1, and f_2 in (2.3), as well as the soft terms, $\mu \to e\gamma$ does not serve as a constraint.

In the last part of section 2.2, we discussed consequences of large neutrino Yukawa couplings assuming U_L to be an identity matrix. We considered two cases: one where neutrino Yukawa couplings are fixed, and the other where boundary condition at M_* is fixed at a universal set of values. Here, let us examine how those results change if we relax the condition on U_L. For the first case, we include l_{ij} into (4.4) to obtain

$$|(\delta^d_{13})_{RR}|^2 + |(\delta^d_{23})_{RR}|^2 \approx |(\delta^l_{13})_{LL} - l_{13}|^2 + |(\delta^l_{23})_{LL} - l_{23}|^2, \tag{4.8}$$

where $(\delta^d_{ij})_{RR}$ and $(\delta^l_{ij})_{LL}$ are at $M_{\rm GUT}$ and $M_{\rm SUSY}$, respectively. Unless l_{ij} is small enough compared to the bound on $(\delta^l_{ij})_{LL} = (\delta^d_{ij})^*_{RR}$ presented in the previous subsection, the limit on the left hand side is appreciably weakened. Note that a model with l_{ij} that large is likely to be ruled out by LFV data. The second case is more promising. One can extend (2.34) in the style of (4.4), to have

$$|(\delta^d_{13})_{RR}|^2 + |(\delta^d_{23})_{RR}|^2 \approx \left(\frac{\alpha}{1+\alpha}\right)^2 \times [|(\delta^l_{13})_{LL}|^2 + |(\delta^l_{23})_{LL}|^2]. \tag{4.9}$$

Therefore, the upper bounds on $(\delta^d_{23})_{RR}$ and $(\delta^d_{13})_{RR}$ attained from (4.4), are further scaled down by $\alpha/(1+\alpha)$.

JHEP11(2008)051

Mixing	Figure		Present	Future
$\lvert(\delta^d_{23})_{RR}(M_{\rm GUT})\rvert$	4	(a)	7.6×10^{-2}–1.4×10^{-1}	1.3×10^{-2}
		(b)	3.8×10^{-2}–7.1×10^{-2}	8.1×10^{-3}
		(c)	1.7×10^{-1}	4.0×10^{-2}
		(d)	8.3×10^{-2}–1.5×10^{-1}	3.9×10^{-2}–4.3×10^{-2}
$\lvert(\delta^d_{13})_{RR}(M_{\rm GUT})\rvert$	5	(a)	2.7×10^{-2}–1.4×10^{-1}	2.5×10^{-3}–1.2×10^{-2}
		(b)	1.6×10^{-2}–7.0×10^{-2}	1.5×10^{-3}–7.3×10^{-3}
		(c)	4.7×10^{-2}	1.1×10^{-2}
		(d)	5.0×10^{-2}	1.1×10^{-2}
$\lvert(\delta^d_{23})_{LL}(M_{\rm GUT})\rvert$	6	(a)	$\mathcal{O}(1)$	$\mathcal{O}(1)$
		(b)	0.6–$\mathcal{O}(1)$	0.3–0.4
		(c)	0.7	0.3
		(d)	0.5	0.3
$\lvert(\delta^d_{13})_{LL}(M_{\rm GUT})\rvert$	7	(a)	0.6	0.3
		(b)	0.6	0.1–0.3
		(c)	0.1	0.06
		(d)	0.1	0.06

Table 5: Upper limit on the size of each mass insertion of down-type squarks at the GUT scale. The second and third columns indicate the values of m_0, $M_{1/2}$, and $\tan\beta$, used in figures 4– 7. Regarding an RR mixing, if there are two numbers separated by a dash, the left one is for $U_L = \mathbf{1}$ and the right one is for $U_L \neq \mathbf{1}$ obeying (2.12). If the two numbers are the same, it is written only once. We do the same for an LL mixing on which the alignment condition is given through U_R instead of U_L. For a general U_R, we drop the $\mu \to e\gamma$ constraint as we do not have a systematic way to impose it.

Recently, an alternative approach to settling down the uncertainties posed by the non-renormalizable operators has been reported [17]. Their work in progress makes use of dependence of the proton lifetime on the coefficients of the operators [26] in order to find a pattern among them. We would say that our strategy is more generic in the sense that it relies only on the condition that the non-renormalizable operators are Planck-suppressed, although it may not be as predictive as their anticipated outcome.

4.3 Summary of bounds

The restrictions on down-type squark mixings at the GUT scale, graphically shown in section 4.1, are condensed in a numerical form in table 5. Each number is the maximum distance of a point from the origin on the corresponding figure that satisfies all the constraints considered in the present work. As for ϕ_{B_s}, we use the DØ result, which is marked in gray (cyan) in figures 4 and 6. We would be left with no solution in many cases if we used the HFAG fit (which would be a very interesting outcome on its own [34, 35, 47, 48]). In order to estimate the power of ϕ_{B_s} measurement at LHCb, we suppose that its future central value will coincide with the SM prediction. We make the same supposition about $\sin 2\beta$.

JHEP11(2008)051

Those upper bounds are subject to change of parameters or scheme of uncertainty treatment. A variation may also be caused by choosing 2×10^{-9} instead of 10^{-8} as the reach of $\tau \to e\gamma$ and $\tau \to \mu\gamma$ searches at a super B factory. In particular, the strength of a LFV constraint depends on U_L and U_R. We take into account the U_L dependence of a maximal RR insertion using the method described in the previous subsection. As for $\mu \to e\gamma$, we suppose Case (a) therein, i.e. we do not envisage a fine tuning among contributions to $(\delta^l_{13})_{RR}$ or $(\delta^l_{23})_{RR}$. If a LFV restriction is important, relaxing the assumption of $U_L = \mathbf{1}$ increases the upper limit of the given insertion. Concerning the limit on an LL insertion, we follow the same procedure to evaluate the dependence of a tau channel on U_R, while we keep $\mu \to e\gamma$ only for $U_R = \mathbf{1}$. Even if U_R is unity, however, it turns out that the leptonic data does not cause a big additional reduction in the bounds set by the hadronic inputs, under the conditions considered in this work. A lepton sector constraint should be looser if we allow for a different U_R. Therefore, the quoted numbers are not greatly influenced by a change of U_R.

4.4 Possible alterations in observables

With the region of each mass insertion obtained in section 4.1, we estimate a possible difference of an affected observable from its SM value. The result is summarized in table 6. Four of them have been already displayed as contours on each figure indicated in the table. Note that what has been shown as contours is the value of the observable, not the deviation from the SM prediction. We use the same set of constraints as in section 4.3.

Under the present conditions, there are still CP asymmetries that might potentially have a discrepancy bigger than the precision attainable at a super B factory. They are $S_{\rm CP}^{K^*\gamma}$, $S_{\rm CP}^{\rho\gamma}$, $A_{\rm CP}^{b\to s\gamma}$, and $A_{\rm CP}^{b\to(s+d)\gamma}$. They show larger possible alterations for higher m_0, while $A_{\rm CP}^{b\to d\gamma}$ doesn't follow this tendency. Being hadronic observables, their sensitivity to the GUT scale flavor violation is amplified for higher m_0, as was explained in section 4.1, although they are more severely restricted by other quark sector processes for the same reason. As we did for table 5, we take account of uncertainties due to a misalignment between quarks and leptons of the lighter two families. In this case, we obtain the values after the dash signs, which can be larger than the estimates for perfect alignment.

We repeat the same task with the prospective future inputs. One may expect the presented deviations, provided that no constraint is seriously violated in a future experiment. With lower m_0, $S_{\rm CP}^{K^*\gamma}$ and $S_{\rm CP}^{\rho\gamma}$ will not show a signature detectable at a super B factory, even if quark-lepton misalignment is allowed, while $A_{\rm CP}^{b\to s\gamma}$ and $A_{\rm CP}^{b\to(s+d)\gamma}$ might reveal a hint. With higher m_0, search for a supersymmetric effect in $S_{\rm CP}^{K^*\gamma}$ becomes feasible as well.

In the case with the $(\delta^d_{13})_{LL}$ mixing, its effect on $A_{\rm CP}^{b\to(s+d)\gamma}$ is negligible so that the variation is at most about 0.5%, because the channel $B \to X_{s+d}\gamma$ is dominated by $B \to X_s\gamma$. We include $S_{\rm CP}^{B_s\to K^*\gamma}$ in the table as well for reference.

Among the CP asymmetries mentioned above, $S_{\rm CP}^{K^*\gamma}$ and $S_{\rm CP}^{\rho\gamma}$ are sensitive to RR mixings of squarks, and thus are closely related to LFV. Recall that RR mixings give rise to much higher LFV rates than LL, as we have seen in section 4.1. This motives us to look into allowed ranges of those two CP asymmetries as functions of LFV branching ratios.

First, we show the correlation between $S_{\rm CP}^{K^*\gamma}$ and $B(\tau \to \mu\gamma)$ in figures 8, each of which results from the same set of mass insertions as the corresponding plot in figures 4.

JHEP11(2008)051

Deviation Mixing	Figure		Present	Future	Future precision
$\left\lvert\Delta S_{\rm CP}^{K^*\gamma}\right\rvert$ $(\delta_{23}^d)_{RR}$	4	(a)	0.04–0.07	0.007	0.02
		(b)	0.04–0.07	0.007	
		(c)	0.18	0.04	
		(d)	0.16–0.26	0.07–0.08	
$\left\lvert\Delta S_{\rm CP}^{\rho\gamma}\right\rvert$ $(\delta_{13}^d)_{RR}$	5	(a)	0.06–0.30	0.006–0.03	0.10
		(b)	0.06–0.28	0.006–0.03	
		(c)	0.21	0.05	
		(d)	0.39	0.09	
$\left\lvert\Delta S_{\rm CP}^{B_s\to K^*\gamma}\right\rvert$ $(\delta_{13}^d)_{RR}$	5	(a)	0.06–0.28	0.006–0.03	
		(b)	0.06–0.28	0.006–0.03	
		(c)	0.17	0.03	
		(d)	0.32	0.05	
$\left\lvert\Delta A_{\rm CP}^{b\to s\gamma}\right\rvert$ (%) $(\delta_{23}^d)_{LL}$	6	(a)	1.3	1.3	0.4
		(b)	1.9–2.3	1.0–1.4	
		(c)	3.3	1.7	
		(d)	5.2	2.8	
$\left\lvert\Delta A_{\rm CP}^{b\to(s+d)\gamma}\right\rvert$ (%) $(\delta_{23}^d)_{LL}$	6	(a)	1.3	1.3	0.6
		(b)	1.8–2.2	0.9–1.3	
		(c)	3.2	1.6	
		(d)	5.1	2.7	
$\left\lvert\Delta A_{\rm CP}^{b\to d\gamma}\right\rvert$ (%) $(\delta_{13}^d)_{LL}$	7	(a)	16	7	
		(b)	57	5–15	
		(c)	7	3	
		(d)	15	6	

Table 6: Maximal departure of each observable from its SM value given the present and the future constraints. The second and third columns indicate the plot on which we calculate the observable. Of the two deviations separated by a dash in a cell, the left one is for $U_L = \mathbf{1}$ and the right one is for $U_L \neq \mathbf{1}$ obeying (2.12), for the first three CP asymmetries. Those two types of deviations should be regarded as the same if only one is written. For the rest, the alignment condition is given through U_R instead of U_L. For a general U_R, we drop the $\mu \to e\gamma$ constraint as we do not have a systematic way to impose it.

Every point on the figures satisfies the current ΔM_{B_s} and $B(B \to X_s\gamma)$ constraints. The upper limit on $\tau \to \mu\gamma$ from $\mu \to e\gamma$ has been deduced from the contours in figures 4. In figures 8 (a) and (b), what restricts $S_{\rm CP}^{K^*\gamma}$ at present is $\tau \to \mu\gamma$, and in the future $\mu \to e\gamma$ at MEG should take over. In figures (c) and (d), d_n, in addition to $\tau \to \mu\gamma$, is playing an important role, and the future expectation of $S_{\rm CP}^{K^*\gamma}$ is determined by ΔM_{B_s} and ϕ_{B_s}. One can find the numerical range of $S_{\rm CP}^{K^*\gamma}$ allowed in each of the four figures in table 6. Note that

JHEP11(2008)051

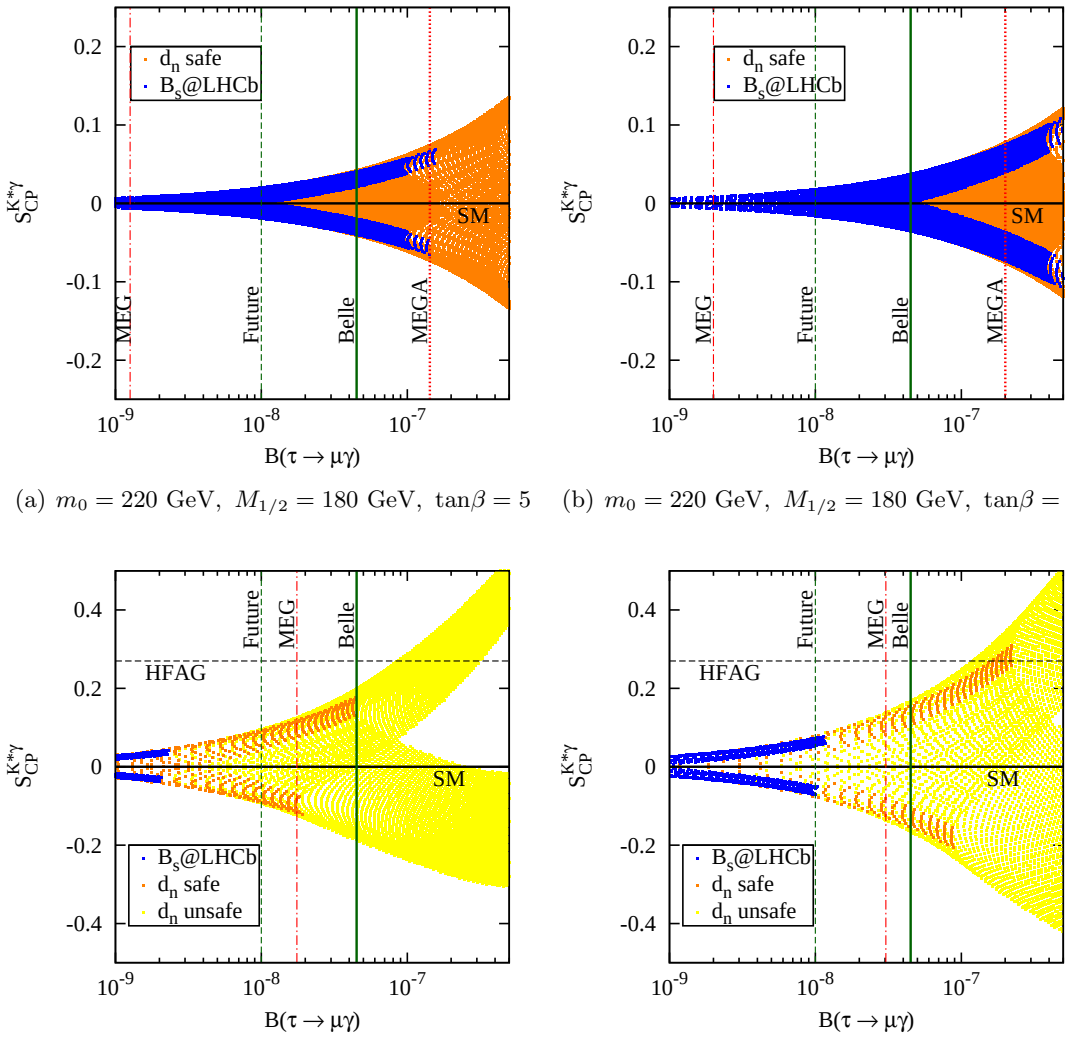

(a) $m_0 = 220$ GeV, $M_{1/2} = 180$ GeV, $\tan\beta = 5$ (b) $m_0 = 220$ GeV, $M_{1/2} = 180$ GeV, $\tan\beta = 10$

(c) $m_0 = 600$ GeV, $M_{1/2} = 180$ GeV, $\tan\beta = 5$ (d) $m_0 = 600$ GeV, $M_{1/2} = 180$ GeV, $\tan\beta = 10$

Figure 8: Correlation between $S_{\rm CP}^{K^*\gamma}$ and $B(\tau \to \mu\gamma)$ obtained by varying $(\delta^d_{23})_{RR}$, with $(\delta^d_{ij})_{LL}$ generated from RG running between the reduced Planck scale and the GUT scale. A light gray (yellow) point is disfavored by neutron EDM, while a gray (orange) point is not, and a black (blue) point satisfies the future ΔM_{B_s} and ϕ_{B_s} constraints. The dashed horizontal line marks the 2 σ range of $S_{\rm CP}^{K^*\gamma}$, and its SM value is the solid horizontal line. The present and the future limits on $\tau \to \mu\gamma$ and $\mu \to e\gamma$ are indicated by the vertical lines.

if two numbers are separated by a dash in the table, one should take the left hand side since the plots are for $U_L = \mathbf{1}$. One could translate these plots to a case where U_L is not fixed at unity, following the prescription presented in section 4.2: regard the horizontal axis as $B(\tau \to (e+\mu)\,\gamma))$ instead of $B(\tau \to \mu\gamma)$, and shift the upper bounds on $\tau \to \mu\gamma$ rightward in accordance to this change, while keeping the positions of the vertical lines for $\mu \to e\gamma$.

Second, let us move to the correlation between $S_{\rm CP}^{\rho\gamma}$ and $B(\tau \to e\gamma)$, displayed in figures 9, which correspond to the parameter space considered in figures 5. We discard any point that is incompatible with the present data of ΔM_{B_d}, $\sin 2\beta$, or $\cos 2\beta$. The upper

JHEP11(2008)051

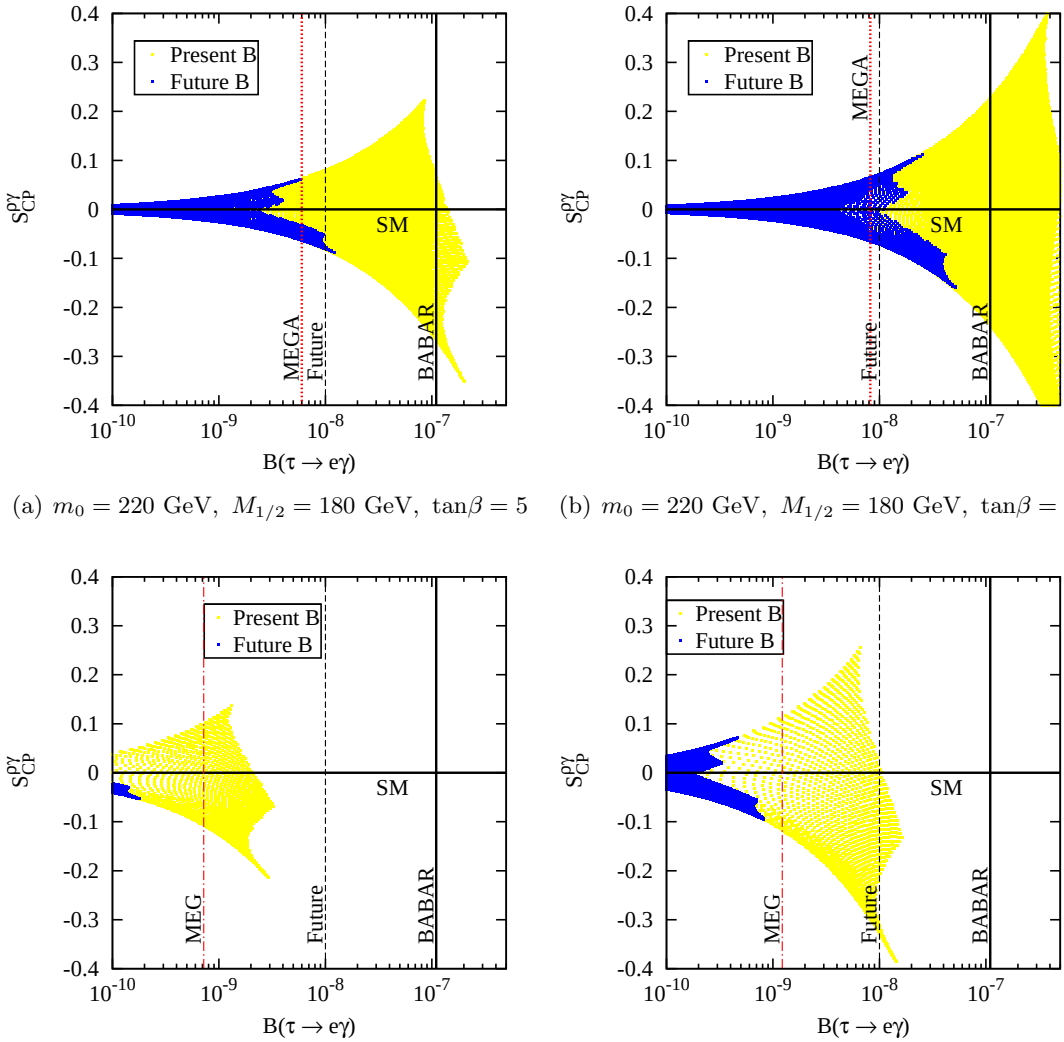

(a) $m_0 = 220$ GeV, $M_{1/2} = 180$ GeV, $\tan\beta = 5$ (b) $m_0 = 220$ GeV, $M_{1/2} = 180$ GeV, $\tan\beta = 10$

(c) $m_0 = 600$ GeV, $M_{1/2} = 180$ GeV, $\tan\beta = 5$ (d) $m_0 = 600$ GeV, $M_{1/2} = 180$ GeV, $\tan\beta = 10$

Figure 9: Correlation between $S_{\rm CP}^{\rho\gamma}$ and $B(\tau \to e\gamma)$ obtained by varying $(\delta^d_{13})_{RR}$, with $(\delta^d_{ij})_{LL}$ generated from RG running between the reduced Planck scale and the GUT scale. A light gray (yellow) point is consistent with all the current constraints, and a black (blue) point satisfies the future ΔM_{B_d} and $\sin 2\beta$ constraints. The solid horizontal line marks the SM value of $S_{\rm CP}^{\rho\gamma}$. The present and the future limits on $\tau \to \mu\gamma$ and $\mu \to e\gamma$ are indicated by the vertical lines. In figures (a) and (b), the MEG line is outside the left border of each plot.

limit on $\tau \to e\gamma$ from $\mu \to e\gamma$ has been inferred as we did in the preceding paragraph. For lower m_0 shown in figures 9 (a) and (b), $\mu \to e\gamma$ provides the limits on $S_{\rm CP}^{\rho\gamma}$ both currently and in the future. The MEG bound is not visible on the plane since it restricts $B(\tau \to e\gamma) \lesssim 7 \times 10^{-11}$. For higher m_0 in figures (c) and (d), possible range of $S_{\rm CP}^{\rho\gamma}$ is determined by the other hadronic observables, with little help from the lepton sector. The way to convert these plots to those for $U_L \neq \mathbf{1}$ is almost the same as above: relabel the horizontal axis as $B(\tau \to (e+\mu)\,\gamma))$ instead of $B(\tau \to e\gamma)$, and change the upper bounds

JHEP11(2008)051

Deviation Mixing	Figure		Present	Future
$\lvert\Delta\phi_{B_s}\rvert$ $(\delta^d_{23})_{RR}$	4	(a)	0.05–0.08	0.01
		(b)	0.02–0.04	0.004
		(c)	0.08	0.08
		(d)	0.05	0.05
$\lvert\Delta\phi_{B_s}\rvert$ $(\delta^d_{23})_{LL}$	6	(a)	0.05	0.05
		(b)	0.02–0.03	0.004–0.008
		(c)	0.57	0.33
		(d)	0.32	0.12

Table 7: Maximal departure of ϕ_{B_s} from its SM value under the present and the future constraints except for those on itself. The second and third columns indicate the relevant plot. Of the two deviations separated by a dash in a cell, the left one is for $U_L = \mathbf{1}$ and the right one is for $U_L \neq \mathbf{1}$ obeying (2.12), for the RR mixing. Those two types of deviations should be regarded as the same if only one is written. In the case with $(\delta^d_{23})_{LL}$, the alignment condition is given through U_R instead of U_L. For a general U_R, we drop the $\mu \to e\gamma$ constraint as we do not have a systematic way to impose it.

on $\tau \to e\gamma$ to those on $\tau \to (e+\mu)\,\gamma$. A difference from the above case is that one should also multiply the $\mu \to e\gamma$ limit on $B(\tau \to e\gamma)$ by $24 \sim \lambda^{-2}$.

The latest interest in the phase of B_s-$\overline{B_s}$ mixing leads us to examine its modification that can be caused by new physics. We lift the constraint on ϕ_{B_s} while keeping the others used in section 4.3, and record its variation allowed by the other bounds in table 7. The difference between the announced central value and the SM prediction is about 0.7. From the table it appears that cases with lower m_0 and/or large RR mixing (but small LL mixing) are disfavored by ϕ_{B_s}. In the case of RR insertion with higher m_0, the primary barrier is the neutron EDM as is evident from figures 4 (c) and (d). Let us remind the reader that this situation can be ameliorated by multiplying $(\delta^d_{23})_{LL}$ by an $\mathcal{O}(1)$ complex factor at $M_{\rm GUT}$. With the LL insertion and higher m_0, on the other hand, figures 6 (c) and (d) show that $B \to X_s\gamma$ and $S^{\phi K}_{\rm CP}$ exclude a major part of the region preferred by the HFAG fit, although there are still remaining parts that are responsible for the large difference in ϕ_{B_s} recorded in the table.

In figures 10, we investigate how LFV constrains ϕ_{B_s} by means of correlation plots, focusing on the RR insertion case considered in figures 4. At first, let us consider only the leptonic constraints. In this case, LFV and the latest ϕ_{B_s} fit are better reconciled for higher m_0 depicted in figures (c) and (d). Obviously, lower $\tan\beta$ is preferable since a LFV limit gets tighter for higher $\tan\beta$. However, if one takes the neutron EDM bound seriously, the light gray (yellow) points are discarded while the gray (orange) points remain, and therefore it becomes harder to account for ϕ_{B_s} with an RR mixing. Remember that one can apply this result to a popular benchmark scenario in which the soft terms at M_* are flavor-blind and all the right-handed squark mixings are supposed to originate from large neutrino Yukawa couplings, as we discussed in the last part of section 2.2. The recipe is to multiply each LFV branching fraction by $(1+\alpha)^2/\alpha^2$ with α in (2.33). This factor arises

JHEP11(2008)051

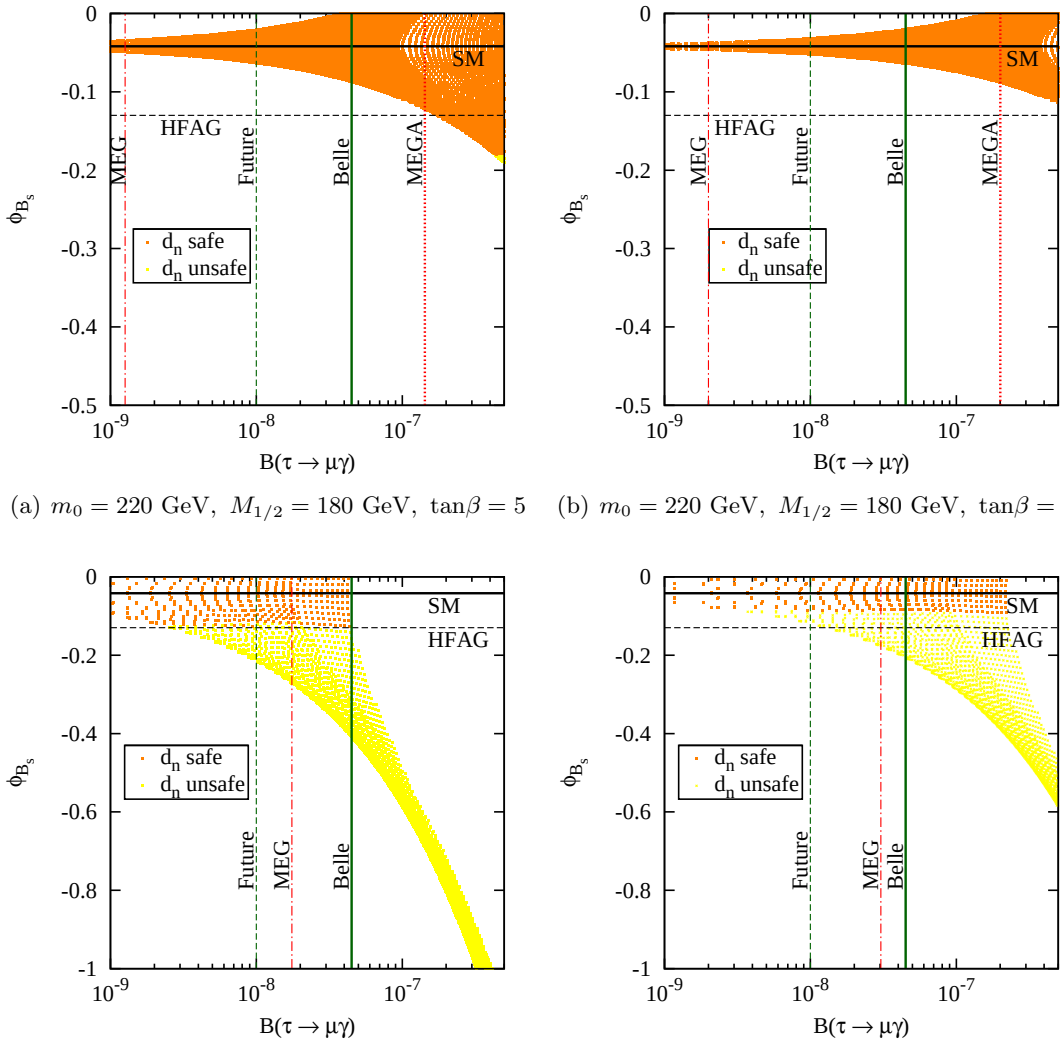

(a) $m_0 = 220$ GeV, $M_{1/2} = 180$ GeV, $\tan\beta = 5$ (b) $m_0 = 220$ GeV, $M_{1/2} = 180$ GeV, $\tan\beta = 10$

(c) $m_0 = 600$ GeV, $M_{1/2} = 180$ GeV, $\tan\beta = 5$ (d) $m_0 = 600$ GeV, $M_{1/2} = 180$ GeV, $\tan\beta = 10$

Figure 10: Correlation between ϕ_{B_s} and $B(\tau \to \mu\gamma)$ obtained by varying $(\delta^d_{23})_{RR}$, with $(\delta^d_{ij})_{LL}$ generated from RG running between the reduced Planck scale and the GUT scale. A light gray (yellow) point is disfavored by neutron EDM, while a gray (orange) point is not. The dashed horizontal line marks the 90% CL range of ϕ_{B_s}, and its SM value is the solid horizontal line. The present and the future limits on $\tau \to \mu\gamma$ and $\mu \to e\gamma$ are indicated by the vertical lines.

from the additional running of slepton masses from $M_{\rm GUT}$ down to M_R, and strengthens LFV as the result.

One can be more optimistic in viewing the same correlation plots. For example, the neutron EDM constraint may be weakened if there is also a non-vanishing complex LL mass insertion at M_*, or one might simply choose to ignore the constraint due to its hadronic uncertainties. Then, it might be that the present status of ϕ_{B_s} is hinting at a LFV process occurring at a rate that can be explored in the near future. Notice that this scenario works best when the value of x defined in (2.26), is around 1/12, as we discussed in section 4.1.

JHEP11(2008)051

5. Conclusions

We imposed hadronic and leptonic constraints on sfermion mixing in a class of supersymmetric models with SU(5) grand unification. We did not particularly assume that the sfermion mass matrices have a universal form at any scale, but rather that any off-diagonal entry may be nonzero, which is generically the case in gravity mediated supersymmetry breaking. Those off-diagonal elements are encoded in the dimensionless mass insertion parameters in terms of which we express experimental bounds on flavor non-universality at the GUT scale. While fixing the gluino mass to 500 GeV at the weak scale, we tried two different boundary conditions on the diagonal components of the soft scalar mass matrix at $M_{\rm GUT}$: lower $m_0 = 220$ GeV and higher $m_0 = 600$ GeV. We varied $\tan\beta$ from 5 to 10 as well. For lower m_0, we have found that the upper limit on an RR mixing is essentially determined by a LFV decay mode both at present and in the near future. This is true even when one introduces non-renormalizable terms to accommodate the lighter down-type quark and charged lepton masses. In particular, the apparently unrelated mode $\mu \to e\gamma$ turns out to be remarkably sensitive to a mixing involving the third family. This sensitivity will be much higher with the progress of the MEG experiment. For higher m_0, the situation turns the other way around so that the hadronic constraints, such as B-meson mixing and neutron EDM, dominate. Also in the near future, measurements at the LHCb and a super B factory, with the aid of improved lattice QCD, should be able to probe an RR mixing, with a sensitivity higher than that of a LFV experiment. Concerning the LL mixings, they are mostly restricted by hadronic data from B physics, although LFV supplies additional information if m_0 is low and $\tan\beta$ is high. These findings unveil a nice complementarity of the quark and the lepton sector processes showing their strengths and weaknesses, depending on the gaugino to scalar mass ratio. We included discussions on the consequences of the discrepancy recently observed in the B_s-meson mixing phase.

Acknowledgments

We thank Sung-Gi Kim, Paride Paradisi, Amarjit Soni, and Diego Tonelli for useful discussions and comments. JhP acknowledges Research Grants funded jointly by the Italian Ministero dell'Istruzione, dell'Università e della Ricerca (MIUR), by the University of Padova, and by the Istituto Nazionale di Fisica Nucleare (INFN) within the *Astroparticle Physics Project*, and the FA51 INFN Research Project, as well as the JSPS postdoctoral fellowship program for foreign researchers and the accompanying grant-in-aid no. 17.05302. This research was supported in part by the European Community Research Training Network UniverseNet under contract MRTN-CT-2006-035863. The work of MY was partially supported by the grants-in-aid from the Ministry of Education, Science, Sports and Culture in Japan, No. 16081202 and No. 17340062.

A. Notations

The scalar mass terms in the soft supersymmetry breaking sector of the minimal supersymmetric standard model are given by

$$-\mathcal{L}_{\rm soft} \supset Q^\dagger m_Q^2\, Q + \overline{U}^T m_U^2\, \overline{U}^* + \overline{E}^T m_E^2\, \overline{E}^* + \overline{D}^T m_D^2\, \overline{D}^* + L^\dagger m_L^2\, L, \tag{A.1}$$

where the uppercase letters denote the scalar components of the SM superfields embedded in T and $\overline{F}$ as in (2.5). Consider a basis where the down-type quark and the charged lepton Yukawa matrices are diagonalized by superfield rotations. The scalars in this basis, denoted by lowercase letters, are related to the above fields by (2.13). Therefore, their mass matrices are connected to those above by the basis change,

$$m_q^2 = m_Q^2, \quad m_u^2 = U_Q\, m_U^2\, U_Q^\dagger, \quad m_e^2 = U_R\, m_E^2\, U_R^\dagger, \quad m_d^2 = m_D^2, \quad m_l^2 = U_L\, m_L^2\, U_L^\dagger. \tag{A.2}$$

Suppose that the squark and slepton mass terms are given by,

$$-\mathcal{L} \supset \widetilde{d}_{Ai}^\dagger\, [m_{\widetilde{d}AB}^2]_{ij}\, \widetilde{d}_{Bj} + \widetilde{e}_{Ai}^\dagger\, [m_{\widetilde{e}AB}^2]_{ij}\, \widetilde{e}_{Bj}, \tag{A.3}$$

in the basis where the down-type quark and the charged lepton mass matrices are diagonal. The sfermion mass matrices include contributions from the Yukawa couplings, the μ term, the D terms, the soft scalar mass terms, and the A terms. In terms of the mass matrices, mass insertion parameters are defined by [30]

$$\begin{aligned} &(\delta_{ij}^d)_{AB} \equiv [m_{\widetilde{d}AB}^2]_{ij}/\widetilde{m}_{\widetilde{d}}^2, \quad (\delta_{ij}^l)_{AB} \equiv [m_{\widetilde{e}AB}^2]_{ij}/\widetilde{m}_{\widetilde{l}}^2, \quad (A,i) \neq (B,j), \\ &(\delta_{ii}^d)_{AA} \equiv (\delta_{ii}^l)_{AA} \equiv 0, \end{aligned} \tag{A.4}$$

where $A, B = L, R$ denote the chiralities, $i, j = 1, 2, 3$ are the family indices, and $\widetilde{m}_{\widetilde{d}}^2$ and $\widetilde{m}_{\widetilde{l}}^2$ are the average sfermion masses [1]. In this work, we heavily rely on the mass insertion notation defined above to discuss the flavor structure of squarks and sleptons. Yet, we do not use mass insertion *approximation* to compute physical amplitudes, but work with mass eigenstates and mixing matrices.

Normally, as its name implies, a mass insertion is a quantity that should be defined at the scale of the particle mass. Therefore, a squark or a slepton mass insertion is considered at the sparticle mass scale or at the weak scale. This is the case in the previous paragraph. In this work, we borrow this notation to deal with the scalar mass matrices at the GUT scale: a GUT scale mass insertion is an off-diagonal entry of a soft scalar mass matrix divided by the averaged diagonal element, in the basis where the Yukawa matrix is diagonal. Following this definition, we have

$$\begin{aligned} &(\delta_{ij}^d)_{LL} = [m_q^2]_{ij}/\widetilde{m}_{\widetilde{d}}^2, \quad (\delta_{ij}^d)_{RR} = [m_d^2]_{ij}/\widetilde{m}_{\widetilde{d}}^2, \\ &(\delta_{ij}^l)_{LL} = [m_l^2]_{ij}/\widetilde{m}_{\widetilde{l}}^2, \quad (\delta_{ij}^l)_{RR} = [m_e^2]_{ij}/\widetilde{m}_{\widetilde{l}}^2, \end{aligned} \tag{A.5}$$

for $i \neq j$.

References

[1] F. Gabbiani, E. Gabrielli, A. Masiero and L. Silvestrini, *A complete analysis of FCNC and CP constraints in general SUSY extensions of the standard model*, *Nucl. Phys.* **B 477** (1996) 321 [hep-ph/9604387].

[2] D0 collaboration, V.M. Abazov et al., *First direct two-sided bound on the B_s^0 oscillation frequency*, *Phys. Rev. Lett.* **97** (2006) 021802 [hep-ex/0603029];
CDF - Run II collaboration, A. Abulencia et al., *Measurement of the $B_s^0 - \bar{B}_s^0$ oscillation frequency*, *Phys. Rev. Lett.* **97** (2006) 062003 [hep-ex/0606027].

JHEP11(2008)051

[3] CDF collaboration, A. Abulencia et al., *Observation of B_s^0–$\overline{B_s^0}$ oscillations*, *Phys. Rev. Lett.* **97** (2006) 242003 [hep-ex/0609040].

[4] Y. Grossman, Y. Nir and G. Raz, *Constraining the phase of B_s-$\overline{B_s}$ mixing*, *Phys. Rev. Lett.* **97** (2006) 151801 [hep-ph/0605028].

[5] D0 collaboration, V.M. Abazov et al., *Measurement of the charge asymmetry in semileptonic B_s decays*, *Phys. Rev. Lett.* **98** (2007) 151801 [hep-ex/0701007]; *Lifetime difference and CP-violating phase in the B_s^0 system*, *Phys. Rev. Lett.* **98** (2007) 121801 [hep-ex/0701012]; *Combined D0 measurements constraining the CP-violating phase and width difference in the B_s^0 system*, *Phys. Rev.* **D 76** (2007) 057101 [hep-ex/0702030];
CDF collaboration, T. Aaltonen et al., *First flavor-tagged determination of bounds on mixing-induced CP violation in $B_s^0 \to J/\psi\phi$ decays*, *Phys. Rev. Lett.* **100** (2008) 161802 [arXiv:0712.2397].

[6] D0 collaboration, V.M. Abazov et al., *Measurement of B_s^0 mixing parameters from the flavor-tagged decay $B_s^0 \to J/\psi\phi$*, arXiv:0802.2255.

[7] M. Ciuchini and L. Silvestrini, *Upper bounds on SUSY contributions to $b \to s$ transitions from B_s-$\overline{B_s}$ mixing*, *Phys. Rev. Lett.* **97** (2006) 021803 [hep-ph/0603114].

[8] M. Endo and S. Mishima, *Constraint on right-handed squark mixings from B_s-$\overline{B_s}$ mass difference*, *Phys. Lett.* **B 640** (2006) 205 [hep-ph/0603251].

[9] J. Foster, K.-I. Okumura and L. Roszkowski, *New constraints on SUSY flavour mixing in light of recent measurements at the Tevatron*, *Phys. Lett.* **B 641** (2006) 452 [hep-ph/0604121];
P. Ball and R. Fleischer, *Probing new physics through B mixing: status, benchmarks and prospects*, *Eur. Phys. J.* **C 48** (2006) 413 [hep-ph/0604249];
S. Khalil, *Supersymmetric contribution to the CP asymmetry of $B \to J/\psi\phi$ in the light of recent B_s-$\overline{B_s}$ measurements*, *Phys. Rev.* **D 74** (2006) 035005 [hep-ph/0605021];
S. Baek, *B_s-$\overline{B_s}$ mixing in the MSSM scenario with large flavor mixing in the LL/RR sector*, *JHEP* **09** (2006) 077 [hep-ph/0605182];
R.L. Arnowitt, B. Dutta, B. Hu and S. Oh, *B_s-$\overline{B_s}$ mixing and its implication for $b \to s$ transitions in supersymmetry*, *Phys. Lett.* **B 641** (2006) 305 [hep-ph/0606130];
B. Dutta and Y. Mimura, *B_s-$\overline{B_s}$ mixing in grand unified models*, *Phys. Rev. Lett.* **97** (2006) 241802 [hep-ph/0607147];
X. Ji, Y. Li and Y. Zhang, *Atmospheric neutrino mixing and $b \to s$ transitions: testing lopsided* SO(10) *flavor structure in B physics*, *Phys. Rev.* **D 75** (2007) 055016 [hep-ph/0612114].

[10] P. Ko and J.-h. Park, *Implications of the measurements of B_s-$\overline{B_s}$ mixing on SUSY models*, arXiv:0809.0705.

[11] A. Baldini et al., *The MEG experiment: search for the $\mu^+ \to e^+\gamma$ decay at PSI*, Research Proposal to INFN, September 2002, http://meg.web.psi.ch/.

[12] S. Baek, T. Goto, Y. Okada and K.-I. Okumura, *Muon anomalous magnetic moment, lepton flavor violation and flavor changing neutral current processes in SUSY GUT with right-handed neutrino*, *Phys. Rev.* **D 64** (2001) 095001 [hep-ph/0104146].

[13] J. Hisano and Y. Shimizu, *GUT relation in neutrino induced flavor physics in SUSY* SU(5) *GUT*, *Phys. Lett.* **B 565** (2003) 183 [hep-ph/0303071].

JHEP11(2008)051

[14] M. Ciuchini, A. Masiero, L. Silvestrini, S.K. VemPati and O. Vives, *Grand unification of quark and lepton FCNCs*, *Phys. Rev. Lett.* **92** (2004) 071801 [hep-ph/0307191].

[15] K. Cheung, S.K. Kang, C.S. Kim and J. Lee, *Correlation between lepton flavor violation and $B_{(d,s)}$-$\overline{B}_{(d,s)}$ mixing in SUSY GUT*, *Phys. Lett.* **B 652** (2007) 319 [hep-ph/0702050].

[16] M. Ciuchini et al., *Soft SUSY breaking grand unification: leptons vs quarks on the flavor playground*, *Nucl. Phys.* **B 783** (2007) 112 [hep-ph/0702144].

[17] F. Borzumati, S. Mishima and T. Yamashita, *Non-CKM induced flavor violation in 'minimal' SUSY* SU(5) *models*, arXiv:0705.2664.

[18] T. Goto, Y. Okada, T. Shindou and M. Tanaka, *Patterns of flavor signals in supersymmetric models*, *Phys. Rev.* **D 77** (2008) 095010 [arXiv:0711.2935].

[19] R. Barbieri and L.J. Hall, *Signals for supersymmetric unification*, *Phys. Lett.* **B 338** (1994) 212 [hep-ph/9408406].

[20] R. Barbieri, L.J. Hall and A. Strumia, *Violations of lepton flavor and CP in supersymmetric unified theories*, *Nucl. Phys.* **B 445** (1995) 219 [hep-ph/9501334];
J. Hisano and D. Nomura, *Solar and atmospheric neutrino oscillations and lepton flavor violation in supersymmetric models with the right-handed neutrinos*, *Phys. Rev.* **D 59** (1999) 116005 [hep-ph/9810479];
L. Calibbi, A. Faccia, A. Masiero and S.K. VemPati, *Running U_{e3} and BR($\mu \to e + \gamma$) in SUSY-GUTs*, *JHEP* **07** (2007) 012 [hep-ph/0610241].

[21] L. Calibbi, A. Faccia, A. Masiero and S.K. VemPati, *Lepton flavour violation from SUSY-GUTs: where do we stand for MEG, PRISM/PRIME and a super flavour factory*, *Phys. Rev.* **D 74** (2006) 116002 [hep-ph/0605139].

[22] UTfit collaboration, M. Bona et al., *First evidence of new physics in $b \leftrightarrow s$ transitions*, arXiv:0803.0659;
For the latest update see e.g. M. Ciuchini, *Some implications of a large phase in B_s mixing*, talk at 5th *International Workshop on the CKM Unitarity Triangle (CKM*2008*)*, Roma Italy September 9–13, 2008, http://ckm2008.roma1.infn.it/.

[23] Heavy Flavor Averaging Group collaboration, E. Barberio et al., *Averages of b-hadron and c-hadron properties at the end of* 2007, arXiv:0808.1297.

[24] J.R. Ellis and M.K. Gaillard, *Fermion masses and Higgs representations in* SU(5), *Phys. Lett.* **B 88** (1979) 315.

[25] H. Georgi and C. Jarlskog, *A new lepton-quark mass relation in a unified theory*, *Phys. Lett.* **B 86** (1979) 297.

[26] D. Emmanuel-Costa and S. Wiesenfeldt, *Proton decay in a consistent supersymmetric* SU(5) *GUT model*, *Nucl. Phys.* **B 661** (2003) 62 [hep-ph/0302272].

[27] T. Moroi, *Effects of the right-handed neutrinos on $\Delta S = 2$ and $\Delta B = 2$ processes in supersymmetric* SU(5) *model*, *JHEP* **03** (2000) 019 [hep-ph/0002208]; *CP violation in $B_d \to \phi K_S$ in SUSY GUT with right-handed neutrinos*, *Phys. Lett.* **B 493** (2000) 366 [hep-ph/0007328].

[28] L.-L. Chau and W.-Y. Keung, *Comments on the parametrization of the Kobayashi-Maskawa matrix*, *Phys. Rev. Lett.* **53** (1984) 1802.

JHEP11(2008)051

[29] Particle Data Group collaboration, W.M. Yao et al., *Review of particle physics*, *J. Phys.* **G 33** (2006) 1.

[30] L.J. Hall, V.A. Kostelecky and S. Raby, *New flavor violations in supergravity models*, *Nucl. Phys.* **B 267** (1986) 415.

[31] F. Gabbiani and A. Masiero, *Superheavy contributions to FCNC in the flipped* SU(5) × U(1), *Phys. Lett.* **B 209** (1988) 289;
J.S. Hagelin, S. Kelley and T. Tanaka, *Supersymmetric flavor changing neutral currents: exact amplitudes and phenomenological analysis*, *Nucl. Phys.* **B 415** (1994) 293.

[32] L. Alvarez-Gaume, M. Claudson and M.B. Wise, *Low-energy supersymmetry*, *Nucl. Phys.* **B 207** (1982) 96.

[33] F. Borzumati and A. Masiero, *Large muon- and electron-number nonconservation in supergravity theories*, *Phys. Rev. Lett.* **57** (1986) 961.

[34] B. Dutta and Y. Mimura, *Large phase of B_s-$\bar{B}_s$ mixing in supersymmetric grand unified theories*, *Phys. Rev.* **D 78** (2008) 071702 [arXiv:0805.2988].

[35] J. Hisano and Y. Shimizu, *CP violation in B_s mixing in the SUSY* SU(5) *GUT with right-handed Neutrinos*, arXiv:0805.3327.

[36] F. Gabbiani and A. Masiero, *FCNC in generalized supersymmetric theories*, *Nucl. Phys.* **B 322** (1989) 235.

[37] S. Baek, J.H. Jang, P. Ko and J.-h. Park, *Fully supersymmetric CP-violations in the kaon system*, *Phys. Rev.* **D 62** (2000) 117701 [hep-ph/9907572]; *Gluino-squark contributions to CP-violations in the kaon system*, *Nucl. Phys.* **B 609** (2001) 442 [hep-ph/0105028].

[38] J. Hisano, T. Moroi, K. Tobe and M. Yamaguchi, *Lepton-flavor violation via right-handed neutrino Yukawa couplings in supersymmetric standard model*, *Phys. Rev.* **D 53** (1996) 2442 [hep-ph/9510309].

[39] P. Paradisi, *Constraints on SUSY lepton flavour violation by rare processes*, *JHEP* **10** (2005) 006 [hep-ph/0505046].

[40] UTfit collaboration, M. Bona et al., *The unitarity triangle fit in the standard model and hadronic parameters from lattice QCD: a reappraisal after the measurements of Δm_s and $BR(B \to \tau\nu_\tau)$*, *JHEP* **10** (2006) 081 [hep-ph/0606167].

[41] M. Nakao, *Probing new physics with rare B, D and K decays*, talk at *Lepton-Photon* 2007, Daegu South Korea August 13–18 2007, http://chep.knu.ac.kr/lp07/htm/S7/S07_21.pdf.

[42] P.G. Harris et al., *New experimental limit on the electric dipole moment of the neutron*, *Phys. Rev. Lett.* **82** (1999) 904.

[43] A. Lenz and U. Nierste, *Theoretical update of B_s-$\overline{B_s}$ mixing*, *JHEP* **06** (2007) 072 [hep-ph/0612167].

[44] V. Lubicz, *CKM fit and lattice QCD*, talk at the 4^{th} *Workshop on Super B-Factory*, Villa Mondragone Frascati Italy November 13–15 2006, http://www.infn.it/csn1/conference/superb/.

[45] M. Bona et al., *SuperB: a high-luminosity asymmetric e^+e^- super flavor factory. Conceptual design report*, arXiv:0709.0451.

[46] M. Neubert, *QCD calculations of decays of heavy flavor hadrons*, arXiv:0801.0675.

JHEP11(2008)051

[47] J.K. Parry and H.-H. Zhang, $B^0_{d,s}$-$\overline{B^0_{d,s}}$ *mixing and lepton flavour violation in SUSY GUTs: impact of the first measurements of* ϕ_s, *Nucl. Phys.* **B 802** (2008) 63 [arXiv:0710.5443].

[48] J.-h. Park and M. Yamaguchi, B_s *mixing phase and lepton flavor violation in supersymmetric* SU(5), arXiv:0809.2614.

[49] G. Wilkinson, *Performance of LHCb with very high statistics*, talk at 1st *LHCb Collaboration Upgrade Workshop*, Edinburgh U.K. January 11–12 2007, http://indico.cern.ch/conferenceDisplay.py?confId=8351.

[50] M. Beneke, G. Buchalla, M. Neubert and C.T. Sachrajda, *QCD factorization for* $B \to \pi\pi$ *decays: strong phases and CP-violation in the heavy quark limit*, *Phys. Rev. Lett.* **83** (1999) 1914 [hep-ph/9905312]; *QCD factorization for exclusive, non-leptonic B meson decays: general arguments and the case of heavy-light final states*, *Nucl. Phys.* **B 591** (2000) 313 [hep-ph/0006124]; *QCD factorization in* $B \to \pi K, \pi\pi$ *decays and extraction of Wolfenstein parameters*, *Nucl. Phys.* **B 606** (2001) 245 [hep-ph/0104110].

[51] G.L. Kane, P. Ko, H.B. Wang, C. Kolda, J.-h. Park and L.T. Wang, $B_d \to \phi K_S$ *CP asymmetries as an important probe of supersymmetry*, *Phys. Rev. Lett.* **90** (2003) 141803 [hep-ph/0304239];
M. Ciuchini, E. Franco, A. Masiero and L. Silvestrini, $b \to s$ *transitions: a new frontier for indirect SUSY searches*, *Phys. Rev.* **D 67** (2003) 075016 [*Erratum ibid.* **D 68** (2003) 079901] [hep-ph/0212397].

[52] G.L. Kane, P. Ko, H.B. Wang, C. Kolda, J.-h. Park and L.T. Wang, $B_d \to \phi K_S$ *and supersymmetry*, *Phys. Rev.* **D 70** (2004) 035015 [hep-ph/0212092].

[53] J. Hisano and Y. Shimizu, *Hadronic EDMs induced by the strangeness and constraints on supersymmetric CP phases*, *Phys. Rev.* **D 70** (2004) 093001 [hep-ph/0406091];
J. Hisano, M. Kakizaki, M. Nagai and Y. Shimizu, *Hadronic EDMs in SUSY* SU(5) *GUTs with right-handed neutrinos*, *Phys. Lett.* **B 604** (2004) 216 [hep-ph/0407169].

[54] MEGA collaboration, M.L. Brooks et al., *New limit for the family-number non-conserving decay* $\mu^\pm \to e^+\gamma$, *Phys. Rev. Lett.* **83** (1999) 1521 [hep-ex/9905013].

[55] BABAR collaboration, B. Aubert et al., *Search for lepton flavor violation in the decay* $\tau^\pm \to e^\pm\gamma$, *Phys. Rev. Lett.* **96** (2006) 041801 [hep-ex/0508012].

[56] S. Hashimoto et al., *Letter of intent for KEK Super B Factory*, KEK-REPORT-2004-4.

[57] Belle collaboration, K. Hayasaka et al., *New search for* $\tau \to \mu\gamma$ *and* $\tau \to e\gamma$ *decays at Belle*, *Phys. Lett.* **B 666** (2008) 16 [arXiv:0705.0650].

[58] BELLE collaboration, Y. Ushiroda et al., *Time-dependent CP-violating asymmetry in* $B^0 \to \rho^0\gamma$ *decays*, *Phys. Rev. Lett.* **100** (2008) 021602 [arXiv:0709.2769].

[59] D. Atwood, M. Gronau and A. Soni, *Mixing-induced CP asymmetries in radiative B decays in and beyond the standard model*, *Phys. Rev. Lett.* **79** (1997) 185 [hep-ph/9704272].

[60] P. Ko, J.-h. Park and G. Kramer, B^0–$\overline{B^0}$ *mixing,* $B \to J/\psi K_S$ *and* $B \to X_d\gamma$ *in general MSSM*, *Eur. Phys. J.* **C 25** (2002) 615 [hep-ph/0206297].

JHEP11(2008)051